High-Order Harmonics- Characterisation, Optimisation and Applications

Lyngå, Claire

1999

High-Order Harmonics

Characterisation, Optimisation and Applications

Claire Lyngå

Lund Reports on Atomic Physics
LRAP-248

Doctoral Thesis
Department of Physics
Lund Institute of Technology
November 1999

ISBN 91-628-3840-7

Contents

Abstract

Recent advances in laser technology, with the development of extremely short-pulse, high-intensity lasers, have opened doors to new areas in atomic physics. By focusing light from an intense, short-pulse laser into a gas jet, the emission of high-order harmonics of the laser frequency has been studied. The aim of this work has been two-fold: to better understand the underlying physics of the harmonic generation process and to demonstrate the use of the generated radiation in novel applications.

Experiments have been performed using both femtosecond and picosecond laser systems. The temporal coherence of harmonic radiation has been measured and characterised. We have shown that the far-field pattern of high-order harmonics separates into two spatial regions with different coherence properties. These features have been related mainly to the single-atom response, but also influenced by different phase-matching conditions. For the central region we find long coherence times, close to the expected duration of the harmonic pulse.

The harmonic spectra from molecular gases have been investigated. They were found to be very similar to those obtained in rare gases, with a plateau and a cutoff whose location is strongly correlated to the ionisation potential. The conversion efficiency in the investigated molecules was not higher than that in one of the rare gases suitable for the specific wavelength region.

Applications using harmonic radiation as a narrowband, coherent XUV source have been performed. Spectroscopic measurements have been made using harmonic radiation produced from a tunable laser source. Lifetimes of highly excited states in CO have been determined and the energy dependence of the photo-ionisation cross-sections of highly excited states in He has been measured. XUV interferometry using harmonic radiation has been demonstrated with femtosecond resolution, using the 11^{th} harmonic of a femtosecond laser, to probe the spatial variation of the electron density in a plasma.

List of papers

Paper I C. Lyngå, A. L'Huillier and C.-G. Wahlström, *High-order harmonic generation in molecular gases,* J. Phys. B **29**, 3293 (1996).

Paper II R. Zerne, C. Altucci, M. Bellini, M.B. Gaarde, T.W. Hänsch, A. L'Huillier, C. Lyngå and C.-G. Wahlström, *Phase-locked high-order harmonic sources*, Phys. Rev. Lett. **79**, 1006 (1997).

Paper III M. Bellini, C. Lyngå, A. Tozzi, M.B. Gaarde, T.W. Hänsch, A. L'Huillier and C.-G. Wahlström, *Temporal coherence of ultrashort high-order harmonic pulses*, Phys. Rev. Lett. **81**, 297 (1998).

Paper IV C. Lyngå, M.B. Gaarde, C. Delfin, M. Bellini, T.W. Hänsch, A. L'Huillier and C.-G. Wahlström, *Studies of the temporal coherence of high-order harmonics*, Phys. Rev. A (to appear 1 Dec, 1999).

Paper V D. Descamps, J.-F. Hergott, H. Merdji, P. Salières, C. Lyngå, J. Norin, M. Bellini, T.W. Hänsch, A. L'Huillier and C.-G. Wahlström, *XUV interferometry measurements with high-order harmonics*, submitted to Opt. Lett.

Paper VI C. Lyngå, F. Ossler, T. Metz and J. Larsson, *A laser system providing radiation tunable from 35 nm to 2 μm*, manuscript for App. Phys. B.

Paper VII P. Cacciani, W. Ubachs, P.C. Hinnen, C. Lyngå, A. L'Huillier and C.-G. Wahlström, *Lifetime measurements of the $E^1\Pi$, v=0 and v=1 states of $^{12}C^{16}O$, $^{13}C^{16}O$ and $^{13}C^{18}O$*, Astrophys. J. **499**, L223 (1998).

Paper VIII M. Gisselbrecht, D. Descamps, C. Lyngå, A. L'Huillier, C.-G. Wahlström and M. Meyer, *Absolute photoionization cross sections of excited He states in the near-threshold region,* Phys. Rev. Lett. **82**, 4607 (1999).

Appendix

Paper IX E. Biémont, C. Lyngå, Z.S. Li, S. Svanberg, H.P. Garnir and P.S. Doige, *Radiative lifetimes, branching fractions and transition probabilities in Ge I – solar implications* , Mon. Not. R. Astron. Soc. **303,** 721 (1999).

Paper X C.M. Sikström, H. Lundberg, G.M. Wahlgren, Z.S. Li, C. Lyngå, S. Johansson and D.S. Leckrone, *New Zr II oscillator strengths and the zirconium conflict in the HgMn star* χ *Lupi*, Astron. Astrophys. **343**, 297 (1999).

1. Introduction

At the beginning of the 20th century atomic physics was in the centre of the research in physics, a position which was later taken over by nuclear and particle physics. However, with the invention of lasers and the rapid development of them, atomic physics has once again become an area of intense research and new discoveries. The laser has given us insight into the fundamental physics of an atom and has become a very useful tool in many fields of atomic physics.

Until recently the atom has been studied by subjecting it to a weak electromagnetic field acting as a perturbation to the field that the electron experiences from the nucleus. The studies have mainly been devoted to mapping the energy levels and radiative properties of the atom in order to understand the physics governing the atom. Recently, with the fast development of high-power lasers it has become possible to subject the atom to electric fields far beyond the field experienced from the nucleus. Under these extreme conditions the physics is of quite a different nature and new phenomena have been discovered. One of these, high-harmonic generation, has attracted a great deal of attention and is the subject of this thesis. Since the discovery in 1987 [1,2] many experiments have been performed and many theories developed to understand the physics behind this process. Briefly, high harmonics are generated when a short, intense laser pulse of linear polarisation interacts with free atoms or molecules. A spectrum of peaks, separated by twice the photon energy of the driving field is produced, as shown in Figure 1.1. The high-harmonic spectrum is characterised by a strong decrease in intensity for the first few orders, after which a plateau is formed by harmonics with approximately the

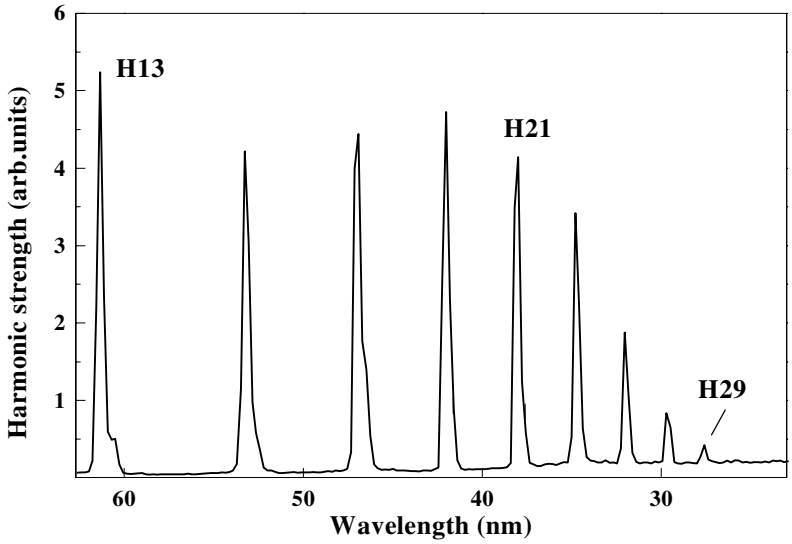

Figure 1.1 *A typical harmonic spectrum generated in argon. The plateau extends until approximately the 21st harmonic where the cutoff begins.*

same intensity. The plateau ends in a sharp cutoff. The interest in harmonic generation is motivated by two reasons: from a fundamental point of view, since it can improve our understanding of the physics governing an atom in a strong laser field; and from an application point of view, since the generated harmonic radiation is a novel source of intense, coherent, short-wavelength radiation.

This thesis is divided into 7 chapters. In this introductory chapter an overview of atoms in strong fields and of the generation of intense, short laser pulses is given. General aspects of harmonic generation are presented in Chapter 2. Chapter 3 deals with the optimisation of the harmonic source, an aspect predominately of interest for applications. The temporal coherence of harmonic radiation is discussed in Chapter 4. Applications using harmonics as a source of short wavelength radiation are discussed in Chapter 5. An outlook regarding possible future developments in the field is presented in Chapter 6. Finally, a few comments are made on the ten papers that are included in the second part of this thesis.

1.1 Atoms in strong fields

This thesis deals with studies made of atoms and molecules in strong fields. A definition follows below of what is meant by a strong field and what characterises these intensities.

The Coulomb field experienced by an electron in the ground state of a hydrogen atom is approximately equal to 5×10^9 V/cm. The relationship connecting the laser intensity (I) and the electric field (E) in a linearly polarised field is given by

$$I = \frac{1}{2}\varepsilon_0 c E^2 \qquad (1.1)$$

where ε_0 is the permittivity of vacuum and c the speed of light. The Coulomb field in a hydrogen atom corresponds to an intensity of 3.5×10^{16} W/cm^2. This intensity is usually referred to as the 'atomic unit of intensity'.

Previously, due to the weak light sources available, it has only been possible to perturb the atom. By disturbing the atom with light much weaker than the force from the nucleus binding the electron to the atom, and studying the decay, it is possible to learn more about the atomic structure. However, as the field increases in strength the atomic states can no longer be considered as unperturbed since they couple strongly to the laser field. With the development of high-power lasers the field of strong-field physics has rapidly evolved and it is now possible to expose atoms to laser fields far beyond that of the atom. In the region where the laser field is comparable to the field binding the electron to the atom, interesting phenomena such as multi-photon processes, above threshold ionisation [3,4], non-sequential multiple ionisation [4] and high-harmonic generation [1,2] have been discovered.

The work in this thesis will concentrate on intensities between 10^{12} W/cm^2 and 10^{15} W/cm^2, which is an interesting region where high-harmonic generation is concerned. Looking into the region where the laser field strongly exceeds the atomic field, relativistic effects become important since the electrons are accelerated to relativistic velocities [5,6]. These effects, which are likely to attract more attention in the near future, will not be addressed here in any detail. Review articles on the interaction between intense laser light and matter are given in [7,8].

The effects we study and which characterise the different intensity regions are strongly related to the motion of the electron. Once the electron is freed by ionisation it will oscillate in the laser field. An important parameter is the ***ponderomotive energy*** which is the average kinetic energy gained by the electron in the laser field. The ponderomotive energy (U_p) or quiver energy, expressed in eV, is given by the following expression:

$$U_p = 9.33 \times 10^{-14} I \lambda^2 \qquad (1.2)$$

where I is the laser intensity in W/cm^2, and λ is the laser wavelength in μm. The ponderomotive energy is also related to the amplitude of the oscillation.

1.1.1 Ionisation

When intense laser light interacts with an atom ionisation is an important factor. Since, generally, the ionisation potential is much greater than the photon energy, a large number of photons are required to ionise the atom. Depending on the laser intensity (and to a lesser extent the ionisation potential of the medium and the laser wavelength) the atom will ionise in different ways. When the intensity is relatively low ***multiphoton ionisation (MPI)*** will occur (Figure 1.2a). MPI is a transition from a bound state to a continuum state by absorption of more than one photon. The multiphoton ionisation model dominates below 10^{14} W/cm^2 for low frequency laser fields (i.e. λ in the near infrared). This value depends on the laser wavelength and species.

At higher intensities the laser field is intense enough to strongly distort the Coulomb potential, making it possible for the electron to tunnel through the barrier formed by the suppressed atomic potential, and ionise (fig 1.2b). This is known as ***tunnel ionisation*** and is dominant for low-frequency lasers at intensities roughly between 10^{14} – 10^{15} W/cm^2. The probability of tunnel ionisation increases with intensity (since this determines the width of the barrier) and wavelength (since this allows more time for the tunnelling process to occur). The ratio of the tunnelling time and the optical period is known as the ***Keldysh parameter*** (γ) and is used to separate the multiphoton region and the tunnelling region [9].

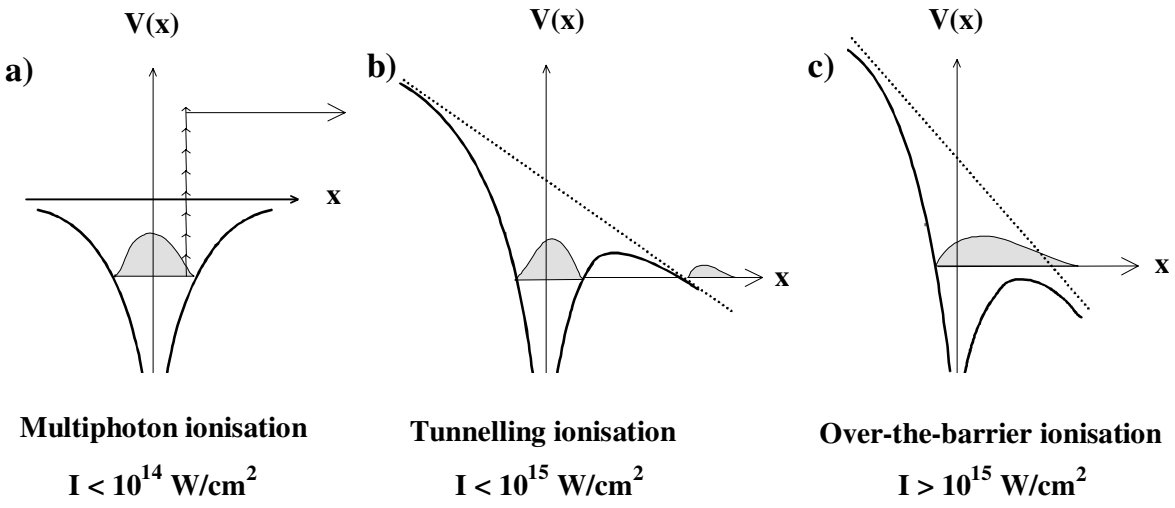

Figure 1.2 *Different ionisation mechanisms for an atom in a laser field. In (a), at intensities below 10^{14} W/cm^2, multiphoton ionisation dominates. As the intensity increases (b) the Coulomb potential is distorted and the electron can tunnel through the barrier. As the intensity is further increased (c) the whole wave packet can escape, due to the barrier being suppressed.*

$$\gamma = \frac{tunnelling\ time}{optical\ period} = \sqrt{\frac{I_p}{2U_p}} \tag{1.3}$$

where I_p is the ionisation potential of the medium. In the low frequency and high-intensity limit ($\gamma<<1$) tunnel ionisation will occur and when $\gamma>>1$ multiphoton ionisation occurs [10]. Naturally, there is not a sharp transition between the two regions, and in many experiments the ionisation mechanism can be considered as a mixture of both. The work in this thesis has been carried out both in the multiphoton region and in the tunnelling region.

As the intensity increases, the barrier becomes lower until finally the ground state is no longer bound. This is known as ***over-the-barrier ionisation*** and is the predominant mechanism for ionisation at intensities above 10^{15} W/cm^2 (Figure 1.2c).

When the field is 'weak' MPI can be modelled by perturbation theory. However, as the field increases in strength and the atomic states couple strongly to the laser field, perturbation theory is no longer adequate. This is particularly true *for* ***above threshold ionisation (ATI)***. ATI is a special case of MPI where more photons than the minimum required for ionisation are absorbed. It was discovered in 1979,

through the occurrence of several distinct peaks in the photo-electron spectrum, separated by the photon energy of the laser [3,4]. Each peak corresponds to a different number of photons absorbed in excess of the ionisation limit. Calculations based on low-order perturbation could not reproduce the observed photo-electron spectra. New non-perturbative approaches had to be developed.

High-harmonic generation is related to ATI, but instead of looking at emitted electrons, photons emitted in the propagation direction of the laser are observed. After the few first harmonics, where the intensity decreases rapidly, a plateau is formed which extends into high photon energies and ends in an abrupt cutoff. This non-perturbative feature was, in the beginning, one of the big question marks in the field. Experimental findings and a theoretical model for harmonic generation are presented in Chapter 2. However, before going into the details of harmonic generation, the lasers required for such generation will be discussed.

1.2 Generation of short and intense laser pulses

The development of strong-field atomic physics has followed that of the available laser intensity at the time. Recent progress in the technology of intense, short pulsed lasers is reflected in the growing number of experiments investigating harmonic generation. The first laser was invented in 1960, and since then this field has seen an explosive development. Many efforts have been made to increase the peak power and focused intensity (for reviews, see [11,12]). A first step to reach higher peak power is to shorten the pulse duration for a given pulse energy. However, non-linear effects and the damage threshold of the optical materials used in the laser ultimately limit the power that can be produced by pulse shortening alone. To allow a further increase in peak power, one way is to expand the laser beam, and thereby reducing the intensity and the non-linear effects. But expansion of the beam requires large optics, which are often very expensive and make the size of the laser very large. An alternative approach is to use the 'CPA-technique', presented below. This is one of three innovations that have dramatically increased the peak power.

The first one is the technique of ***Q-switching***, where by blocking the laser cavity a large population inversion can be built up. When the cavity is opened the accumulated population inversion is dumped in one large short pulse, typically a few tens of nanoseconds long.

In the second technique, ***mode locking***, several longitudinal modes of the laser are made to oscillate in phase. By locking the phases together all the longitudinal modes will reach their maximum at the same time. The field will add constructively forming a train of intense pulses with a time separation corresponding to the cavity round-trip time. The width of the gain profile determines how many modes the cavity can support and consequently how short the pulse can be. Ideally,

$t_p \, \Delta\nu = 0.44$ for a Gaussian pulse, where t_p is the pulse length and $\Delta\nu$ is the bandwidth. Both Q-switching and mode locking are attained by adding an active or passive component in the laser cavity. Both these techniques have resulted in a shortening of the pulse length, from which the increase in intensity follows.

The third technique, ***chirped pulse amplification (CPA)*** [13], is a technique where the pulse is stretched in time (typically a few thousand times) before amplification. This lowers the intensity of the pulses by the same factor and they can be amplified using small-scale optics. Finally, after amplification, the beam is expanded and the pulse is compressed in time back to the original pulse length. The subtlety of this scheme, illustrated in Figure 1.3, lies in stretching the pulse in a controlled way so that it can be compressed back to its initial length after amplification. This is done by taking advantage of the broad spectrum that is inherent in short pulses. (According to the Heisenberg uncertainty principle a pulse with a length of 100 fs must have a bandwidth of around 10 nm at a laser wavelength of 800 nm.) After the oscillator the pulse is stretched in a dispersive delay line so that the red (long wavelength) part of the bandwidth travels first and the blue (short wavelength) part travels on the trailing edge. This produces a chirped pulse, i.e. a pulse with a time-dependent frequency. The stretching can be done taking advantage of group velocity dispersion in an optical fibre, diffraction in a pair of gratings or dispersion in a pair of prisms. Once the amplification is accomplished the pulse is re-compressed in such a way that the red light travelling first has to propagate a longer optical distance, thus creating a short unchirped pulse with very high intensity. Central to this technique is that the amplification is uniform over the whole pulse, otherwise different frequencies will be amplified differently and the pulse can no longer be compressed to a Fourier transform limited pulse. This makes titanium sapphire (Ti:sapphire) a very suitable material for amplification since it has the

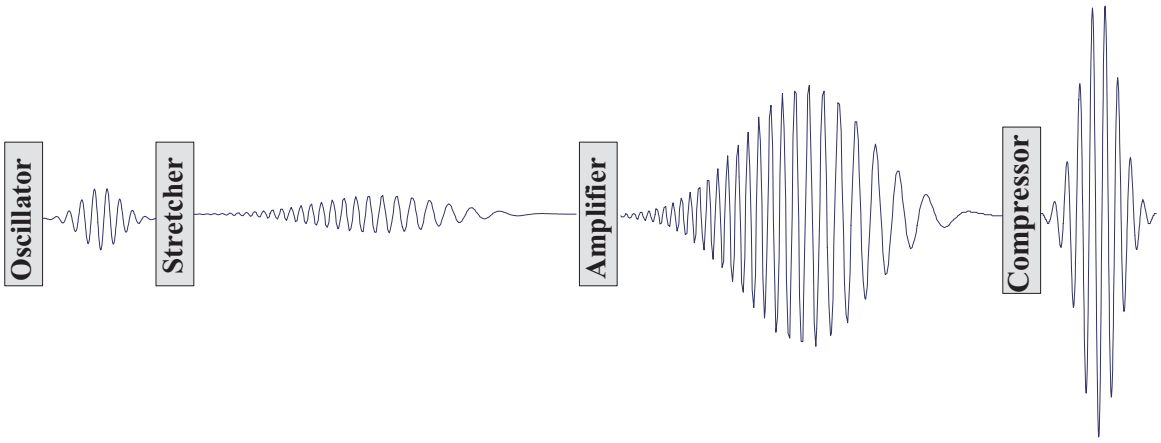

Figure 1.3 *The basic principle for chirped pulse amplification. Initially the pulse is stretched in time, then it is amplified and finally compressed back to its initial pulse length.*

broadest known gain profile (FWHM 230 nm) [11]. Ti:sapphire can support pulses down to approximately 4 fs at 800 nm. This material has the advantage of a high saturation fluence (≈ 1 J/cm^2) and high damage threshold (≈ 8-10 J/cm^2) [11]. It also has a large absorption maximum around 500 nm, making pumping by frequency doubled Nd:YAG lasers ideal.

Chirped pulse amplification has made it possible to generate ultra-high intensities with relatively small laser systems. Together with Ti:sapphire as a gain medium compact T^3 (**T**able-**T**op **T**erawatt) laser systems have been developed. They are now available in many laboratories throughout the world and have enabled the study of strong-field physics to be conducted at several moderately sized universities and research institutes.

In this thesis results are presented from experiments performed at the Lund High-Power Laser Facility [14], using two different laser systems. The choice of system depends on the requirements and goal of the experiment. The most powerful laser is a 10 Hz, 100 fs, terawatt laser, which is a CPA based Ti:sapphire laser system. This laser has recently been upgraded and a new high-power arm of the laser implemented. This is operated in parallel with the original arm, and is designed to deliver pulses with a peak power of up to 10 TW (1 J/pulse). However, the experiments described in this thesis have been performed using the original arm, delivering a peak power of 2.5 TW. The pulse length was 100-150 fs long with an available pulse energy of 250 mJ. This system has been used in the experiments described in Papers I, IV and V, where the high intensities and short pulses are essential.

In Papers II, VI, VII, VIII, IX and X results obtained with a 10 Hz picosecond laser system are presented. This system produces laser light ideal for spectroscopy: tunable, of narrow bandwidth and of relatively short pulse length. The pulse length is of course related to the bandwidth through the Heisenberg uncertainty relation and, as a consequence, the pulse length should not be too short. This system has mainly been used for spectroscopic applications and is presented further in Chapter 5 and in Paper VI.

Paper III describes an experiment performed at LENS (European Laboratory for Non Linear Spectroscopy) in Florence, Italy. In this experiment we used a 100 fs Ti:sapphire laser with a higher repetition rate (1 kHz) but lower peak power than the Lund system.

2. High-order harmonic generation: General aspects

2.1 Typical experimental setup

A typical experimental setup for harmonic generation is illustrated in Figure 2.1. The laser is focused by a lens into a vacuum chamber, where it interacts with a pulsed gas jet containing the non-linear medium. For the work in this thesis a focal length between 15 cm and 1 m was used. It is important to keep a low background pressure (between 10^{-5} and 10^{-4} mbar) for different reasons. Firstly, radiation below 200 nm (vacuum ultra violet radiation, VUV) is absorbed in air. Secondly, the very high intensities achieved when focusing the laser beam can cause degradation of the beam if focused in air, due to the non-linear index of refraction. Finally, the detectors should be stored and operated in vacuum. The number density in the gas jet is usually 10^{17} - 10^{18} atoms/cm^3 (4-40 mbar). The pulsed gas jet is synchronised with the laser and opens 1 ms before the pulse arrives and closes immediately after it. The diameter of the nozzle is typically 1 mm. This corresponds approximately to the length of the interaction region since the focus is usually placed just below the nozzle. In the interaction between the strong field and the atoms, odd harmonics of the laser frequency are created. The laser beam and the harmonics propagate in the same direction and a spectrometer is usually used to separate the different harmonic orders. Using a conventional spectrometer with an entrance slit followed by a grating means that the entrance slit has to be placed close to the gas jet to obtain a large collection efficiency. However, at this position the fundamental beam is still small and will cause damage to the slit. To avoid this, a spectrometer without a slit is used and the gas jet is placed in the position of the slit. The diverging laser beam must expand enough not to damage the grating. In our case, the distance to the grating from the interaction region was always longer than the focal length of the lens. Hence, the power density on the grating was not larger than that of the

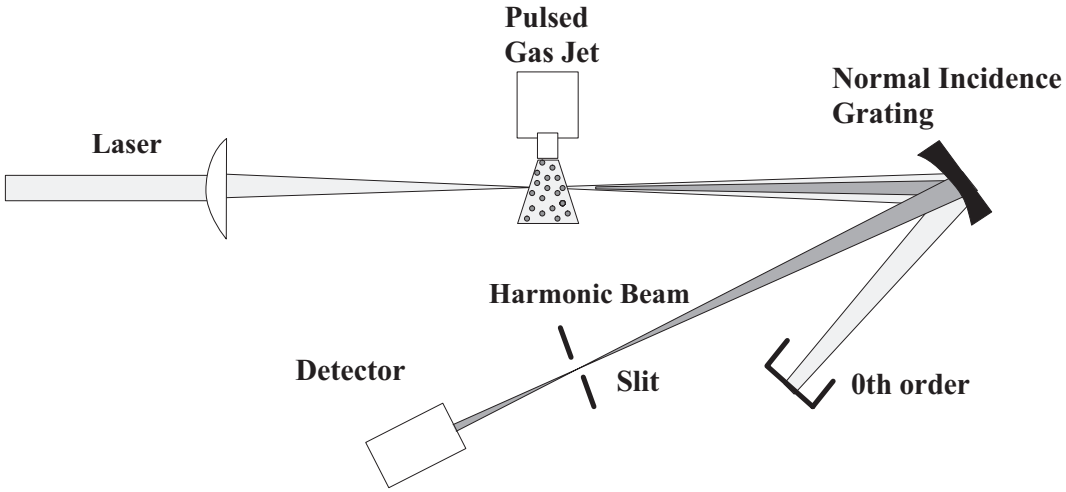

Figure 2.1 *Experimental setup for harmonic generation using a normal incidence grating.*

unfocused beam. In the figure a normal incidence grating is drawn, which is suitable for lower orders. Such a grating has been used in most of the experiments described in this thesis (Paper II, IV, V, VI, VII and VIII). The grating has a radius of curvature of 1 m, thereby eliminating the need for a separate focusing mirror and increasing the total reflectivity of the system. The grating is gold coated, optimised for 70 nm with 1200 grooves/mm. For higher orders a grazing incidence grating should be employed since the efficiency of the normal incidence grating is too low. Astigmatism is much increased with a grazing incidence grating. The harmonics are detected using, for example, an electron multiplier tube (EMT) or a micro channel plate (MCP).

2.2 Experimental findings

2.2.1 Laser related effects

When the laser intensity is low, the strength of the harmonics follows the predictions of perturbation theory and the strength decreases rapidly with increasing order. Once the laser intensity is increased a plateau starts to form where the harmonics have approximately the same intensity. The extent of the plateau grows with increasing laser intensity. The harmonic efficiency decreases rapidly at the cutoff, which marks the end of the plateau. The plateau can extend into very high photon energies. Most of the effort after the discovery of high-order harmonics was put into studying the physics behind the plateau and the extent of it [15-17]. The position of the cutoff was found theoretically to be [18]

$$E_{cutoff} = I_p + 3.2U_p \qquad (2.1)$$

where I_p is the ionisation potential of the medium in the gas jet and U_p is the ponderomotive energy ($U_p \sim I\lambda^2$). Therefore, to achieve very high harmonics a low frequency laser should be used and a high laser intensity. However, the maximum intensity that the atom can experience is I_{sat} which is the saturation intensity. Beyond this the atom will ionise and no further harmonic emission will be possible. This means that for the generation of short wavelengths, atoms with a high ionisation potential (for example helium and neon) are desirable both because of the high I_p and also because of their high saturation intensity. The pulse length of the laser is also of importance here since with extremely short laser pulses the atoms can survive to very high intensities without being ionised. The development of femtosecond lasers has made it possible to generate pulses of only a few optical cycles, thus exposing the atoms to extremely high intensities. This has attracted a lot of attention in the last few years and will be discussed more in Chapter 3 where optimisation of the photon energy is addressed. It should be added that Equation 2.1 is based on the single-atom response. When describing harmonic generation theoretically, we have to combine single-atom theory that describes the response from one single atom to the laser field, with a macroscopic model that accounts for

phase matching and other propagation effects. Achieving good phase matching is one of the challenges in harmonic generation and will be discussed further in Chapter 3.3. When propagation effects are taken into account the factor 3.2 is reduced, depending on focusing conditions and intensity, to around 2 [17].

In Figure 2.2 the intensity dependence of the 13th harmonic in xenon is shown. At low intensity, when the harmonic is in the cutoff, the efficiency increases rapidly with increasing intensity. The slope for different harmonics increases with increasing harmonic order. Once the harmonic reaches the plateau the slope decreases and is similar for different harmonic orders. Finally, as the saturation intensity is reached the medium starts to ionise and the harmonic yield will also saturate.

The influence of the laser polarisation on harmonic generation was studied in [19]. A strong dependence of the harmonic strength on the ellipticity of the laser was found. The maximum signal was obtained for linearly polarised light with the harmonic efficiency decreasing with ellipticity. The decrease of harmonic strength was steeper for high-order harmonics.

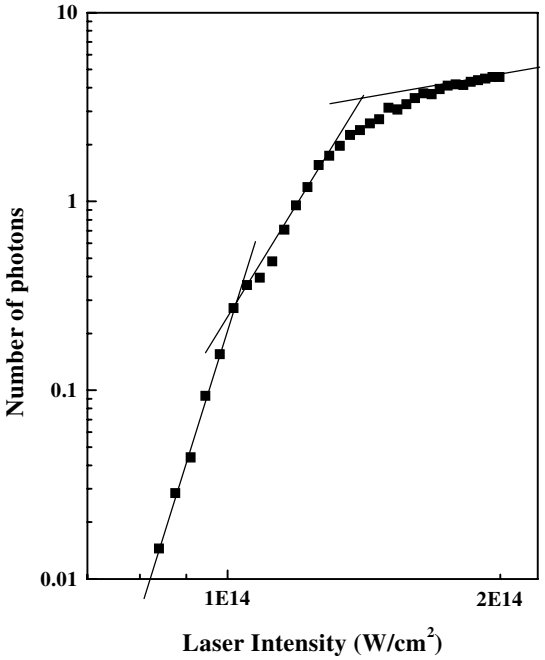

Figure 2.2 *Photon yield of the 13th harmonic generated in xenon, as a function of laser intensity. At low intensities, the harmonic is in the cutoff region and the efficiency increases rapidly with intensity. When the harmonic becomes part of the plateau the slope decreases and finally saturation is reached when the medium starts to ionise.*

2.2.2 The non-linear medium

Most investigations have been performed using rare gases as the non-linear medium. Figure 2.3 shows schematically how the conversion efficiency of the harmonic generation varies with static polarisability and ionisation potential. Atoms that are easily polarisable are very efficient for harmonic generation. However, the plateau cannot be extended as far as with the atoms having a high ionisation potential. For the rare gases the static polarisability increases with atomic number and the ionisation potential decreases. The relationship between static polarisability and ionisation potential can be understood from the fact that the polarisability is a measure of how easily the electron cloud is polarised. This is obviously easier when the electrons are more loosely bound. From this relationship the question arises whether molecules, that can have a very high static polarisability, would be a more efficient source of harmonic radiation. This was investigated in Paper I and is further discussed in Chapter 3. The non-linear medium is not limited to atoms and molecules [20, Paper I], high-order harmonics can also be created in ions [21], clusters [22] and solid targets [23,24].

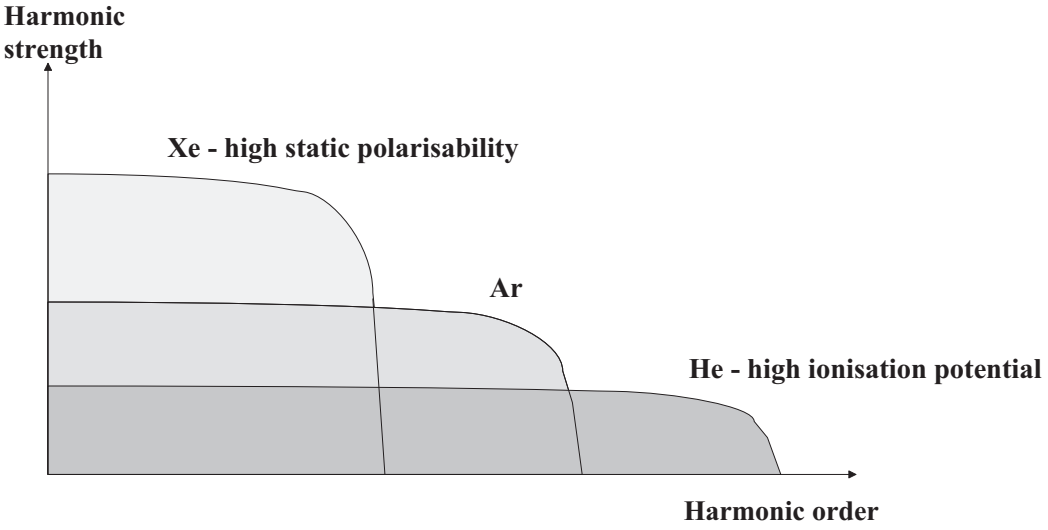

Figure 2.3 *Schematic figure of the harmonic strength when generated in different rare gases. Heavy atoms with a large static polarisability make an efficient medium for low order harmonics. Atoms with a high ionisation potential can be used to generate higher harmonic orders.*

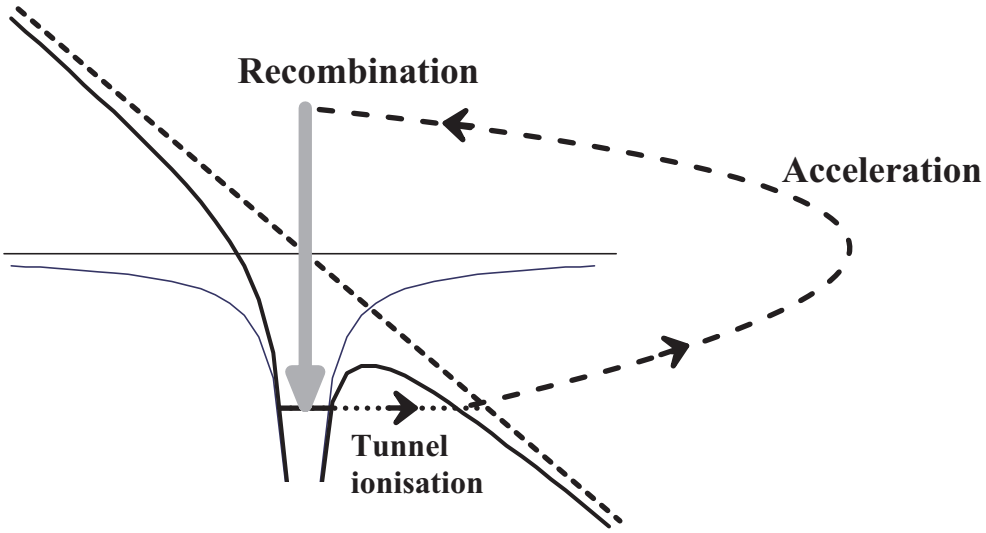

Figure 2.4 *Description of the harmonic generation process according to the semi-classical model. The three different stages are a) tunnel ionisation of the electron, b) acceleration of the electron in the laser field and c) recombination to the ground state.*

2.3 Semi-classical model

A major breakthrough in the understanding of harmonic generation was achieved with the development of the ***semi-classical model*** by Schafer *et al.* [25] and Corkum [26]. This model presents a very intuitive picture of harmonic generation and is capable of explaining, at least qualitatively, many experimental results. The model consists of three different stages. The potential experienced by an atom in the ground state, at one time in the laser period, is displayed in Figure 2.4. The undisturbed Coulomb potential is marked with a thin solid line, the superimposed laser field with a dashed line and the resulting potential by a thick solid line. In the first stage, the Coulomb potential is deformed by the strong laser field according to the figure, and a barrier is formed through which the electron can tunnel. The free electron is born in the laser field with zero velocity. Once liberated from the ion core, the electron is accelerated by the laser field. When the field changes sign the electron is decelerated and may be driven back to the core, where it can recombine to the ground state. The kinetic energy gained in the laser field is emitted as a high-energy photon. The maximum kinetic energy an electron can have when it returns to the core is 3.2 U_p. This explains the dependence of the extent of the plateau, on laser intensity and wavelength, found experimentally ($U_p \sim I \lambda^2$). This process is repeated every half cycle. This is why only odd harmonics are created. Since we have a symmetric medium there is a periodicity of T/2, corresponding to a periodicity of 2ω in frequency. (Should an asymmetric medium be used it should be possible to see even harmonics.)

This model predicts a strong dependence on the polarisation of the driving laser field. For harmonics to be emitted, the classical electron trajectories have to pass close to the nucleus so that the electron can recombine to the ground state. This can only happen with linear polarisation and, consequently, the harmonic efficiency should be strongly ellipticity dependent. This explains the experimental results mentioned earlier. However, Budil *et al.* [19] found that the harmonic generation does not abruptly cease once the polarisation is elliptical, as is predicted by the semi-classical model. To explain this we have, as is more correct, to describe the electron as a wave packet rather than a point charge. This wave packet spreads transversely as it moves in the continuum. Therefore, even if the centre of the wave packet misses the nucleus, there is still a possibility for recombination.

We shall return to the semi-classical model later and discuss in more detail different trajectories that the electron follows in the continuum and the implications on the harmonic emission. Several of the experimental results can be explained using this simple model.

3. Optimisation of high-order harmonics

Optimisation of the harmonic efficiency at a specific wavelength is a key issue when harmonic radiation is used in applications. After the discovery of harmonic generation the first obvious challenge was to generate as short wavelengths as possible. This was pursued by a number of groups; in 1993 Macklin *et al.* [15] observed harmonics up to the 109^{th} order by using a 806 nm laser; L'Huillier *et al.* [16] reached harmonics up to the 135^{th} harmonic in neon using a 1053 nm laser and in 1996 Preston *et al.* [27] produced the 37^{th} harmonic using a 248 nm laser. In 1997, the biologically interesting wavelength region of 2.3-4.4 nm was reached using harmonic orders exceeding 200 [28,29]. This is the so-called 'water window' where oxygen is less absorbing than carbon, which is interesting for imaging of protein rich materials in wet samples. These advances have been made possible by the development of extremely short laser pulses. The emission of harmonic radiation is limited by ionisation. The saturation intensity (I_{sat}) [30] is the laser intensity where the probability of ionisation during the laser pulse is equal to one. I_{sat} depends both on the atomic species and the pulse length. The ionisation rate is low for the light rare gases (high I_p) and they will therefore survive to higher intensities than the heavier rare gases. Decreasing the pulse length increases I_{sat} further, since ionisation has less time to take place. The laser pulses used in [29] to reach the water window were only 5 fs long, which corresponds to only 2 optical cycles (at 780 nm). The number of photons generated with such extremely short wavelengths were, however, very few and the practical use of the radiation is limited at this stage. To make harmonic generation a realistic source in this wavelength region, a way will have to be found to increase the photon number significantly. The aim in the work presented in this chapter, and in Paper I, has not been to generate as short wavelengths as possible, but rather to optimise the number of photons at a certain wavelength.

In this chapter, the optimisation of the harmonic yield for a certain wavelength region with respect to a few parameters is discussed. Important parameters are; the focusing conditions, the non-linear medium, the wavelength of the driving field and the pressure in the gas jet. We will start by discussing effects related to the single-atom response, that is, the laser wavelength and the properties of the non-linear medium (e.g. ionisation potential and static polarisability). Following this, macroscopic effects related to the propagation of the field are treated. These include phase matching, focusing geometry and pressure in the gas jet.

3.1 Influence of the wavelength

The cutoff equation (2.1) does not provide any information on the efficiency of the harmonic process for a harmonic in the plateau. Studies have shown that the efficiency is related to the laser wavelength, a shorter wavelength of the driving

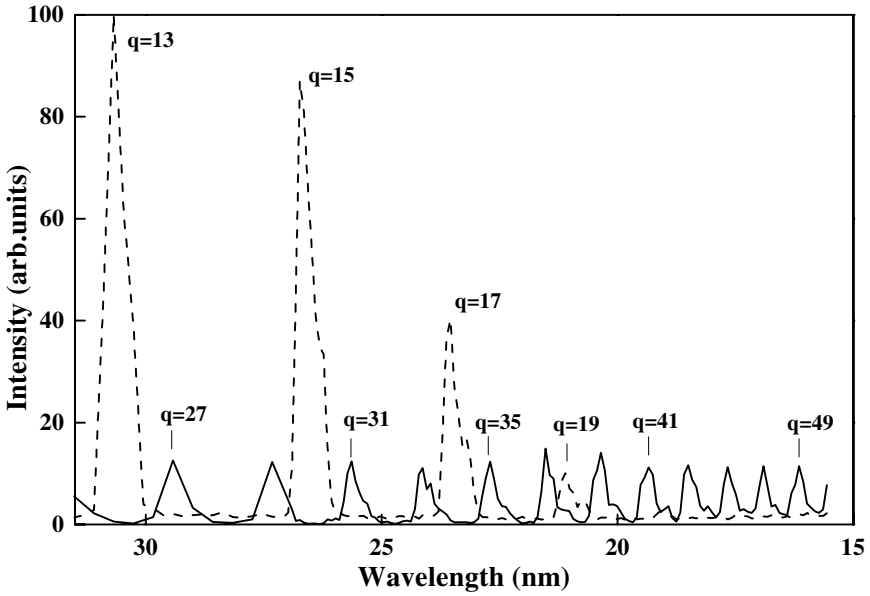

Figure 3.1 *Comparison between harmonic radiation generated with the fundamental frequency, 800 nm (solid curve), and the doubled frequency, 400 nm (dashed curve).*

field giving higher conversion efficiency [31,32]. Although the extent of the plateau will be reduced, for applications requiring only modestly high photon energies it might be possible to increase the harmonic photon yield by changing the fundamental laser frequency. We have compared the amount of photons generated in neon with the fundamental of the Ti:sapphire laser (800 nm) and the doubled frequency (400 nm). The comparison is made for the specific conditions of our setup and aims at demonstrating two approaches for generating a specific wavelength. The laser frequency is doubled with a KDP crystal with approximately 40 % efficiency. The comparison is made keeping the fundamental laser energy constant; consequently the harmonics generated with the frequency-doubled light are generated with considerably less energy. From the results in Figure 3.1 we conclude that the advantage of using the doubling crystal depends on the wavelength region of interest. In our conditions it is clearly beneficial to first double the laser frequency, when wavelengths above 27 nm are generated, whereas below this wavelength the fundamental should be used. In agreement with our expectations, the plateau generated with the longer laser wavelength extends much further. It should be noted that when using the doubled frequency, the beam only contains 40 % of the energy, but the focus spot will be smaller due to the shorter wavelength. In Paper VIII the procedure of first doubling the laser frequency and then generating harmonics was employed. However, this was not done to increase the yield but to generate an 'even' harmonic (the 14^{th}), needed for the spectroscopic

application. The 7th harmonic of the doubled fundamental was instead generated. An intuitive explanation for the efficiency dependence on the wavelength can be attained by returning to the semi-classical model. The time the electron spends in the continuum is proportional to the wavelength. As the electron is accelerated in the continuum the wavefunction spreads transversely. This means that for long wavelengths the wavefunction will be more spread out when is passes the core. Consequently, the recombination probability decreases and the harmonic yield becomes lower.

3.2 The non-linear medium

3.2.1 Atoms and ions

Most of the early work on harmonic generation was performed with rare gases as the non-linear medium [15,17,32,33]. The extent of the plateau was found to be strongly dependent on the ionisation potential and the cutoff formula was derived. Very high-order harmonics, with orders exceeding 100, are generated only in the light rare gases (Ne, He) having high ionisation potentials. A natural extension of these studies consisted in studying ions, which can have an even higher ionisation potential. The response from ions, however, was found to be very weak compared to the neutral response [17,27]. In some cases the cutoff came earlier than predicted by the cutoff law [21]. This was attributed to ionisation-induced defocusing of the fundamental beam, due to the large number of free electrons created.

3.2.2 Molecules

Figure 2.3 in Chapter 2 shows schematically how the efficiency of the rare gases is related to ionisation potential and static polarisability. For the rare gases the conversion efficiency is directly related to static polarisability, the maximum efficiency being for xenon with the highest static polarisability. Considering the high static polarisability that some molecules exhibit, the question is raised whether they will be a more efficient source for harmonic radiation. This is of interest for applications since it might be a way to increase the number of photons at a certain wavelength. Due to the relatively low ionisation potential one cannot expect to obtain very short wavelengths, but the harmonic yield of moderately high harmonics might be increased. Studies by Liang *et al.* [20] have shown that for some diatomic molecules (H_2, D_2, N_2 and O_2) the conversion efficiency increases with static polarisability. If this is the case for all molecules it should be possible to obtain even higher efficiencies by choosing a molecule with very high static polarisability. In the experiment described in Paper I harmonic generation was studied in a number of molecular gases, chosen because of their large span of ionisation potentials, static polarisabilities and different molecular structure. The aim was to correlate the properties of the gases to the harmonic spectra obtained.

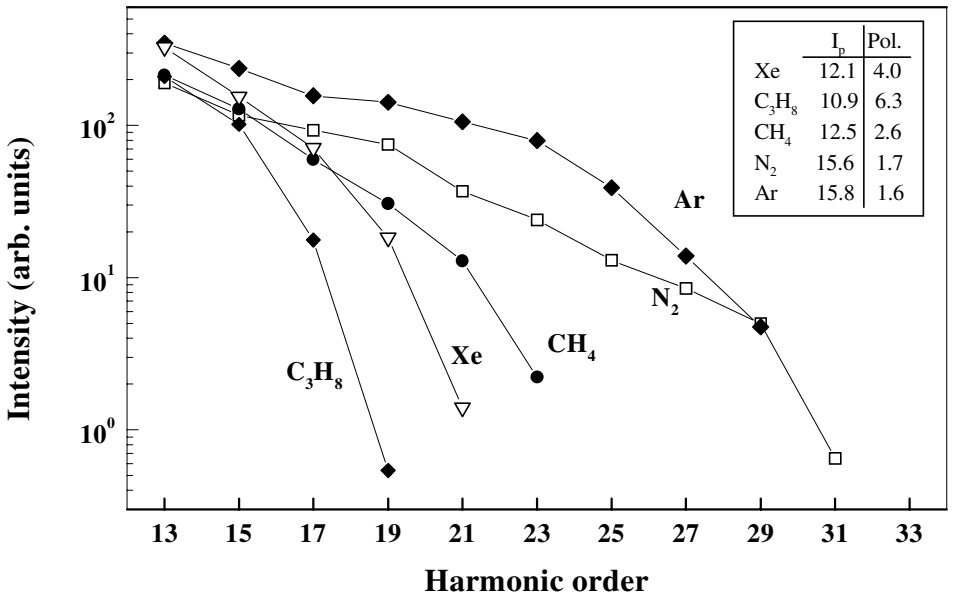

Figure 3.2 *Harmonic spectra generated in different atomic and molecular gases. The extent of the plateau increases with increasing ionisation potential. The ionisation potential, I_p (eV), and static polarisability, Pol., (10^{-24} cm^3) are given in the table.*

The harmonic spectra presented in Figure 3.2 show how the extent of the plateau increases with increasing ionisation potential in the same way as for the rare gases. C_3H_8 has a higher static polarisability than Xe but it is still less efficient. In Figure 3.3 spectra obtained from a rare gas (Ar), a diatomic molecule (N_2) and a larger molecule (SF_6) are compared. The gases have approximately the same ionisation potential. Ar and N_2 present similar behaviour, with respect both to the extent of the plateau and harmonic efficiency. The intensity of the harmonics in SF_6 decreases continuously until the 17th harmonic. Harmonics are produced with a low efficiency but are present until the 31st harmonic. One explanation for this behaviour is that the molecule dissociates early during the laser pulse so that harmonics are produced from fragments and not from the SF_6 molecule. To investigate this further we recorded time-of-flight (TOF) measurements in similar conditions. In the TOF spectrometer the ions are accelerated in an electric field before they are detected. The flight time is directly related to the mass and charge of the ion and consequently species with different mass and charge will be resolved. The time-of-flight spectrum, shown in Figure 3.4, displays SF_5^+, SF_4^+, SF_3^+, SF_2^+, SF^+, S^+ and F^+. There is no trace of SF_6^+, supporting the idea that the harmonics might be generated in the atomic or molecular fragments, and not in SF_6. Fluorine (F) has a high ionisation potential of 17.4 eV and sulphur (S) has a low ionisation potential of 10.4 eV. The long plateau and low photon yield indicates that the highest harmonics are generated in atomic fluorine; the efficient generation of lower harmonics can then be attributed to sulphur. However, this

interpretation does not explain the dip around the 17th harmonic. Results from more molecular gases are presented in Paper I. Summarising the results, we find that the rare gases are still the most efficient medium despite the higher static polarisability exhibited by some of the molecules.

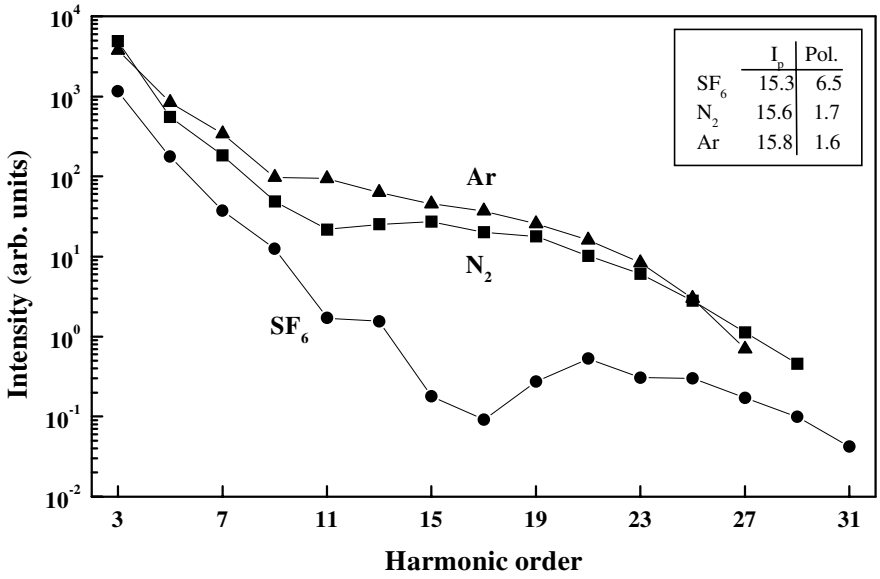

Figure 3.3 *Comparison of the harmonic spectra of three different gases with approximately the same ionisation potential. The ionisation potential, I_p (eV), and static polarisability, Pol., (10^{-24} cm^3) are given in the table.*

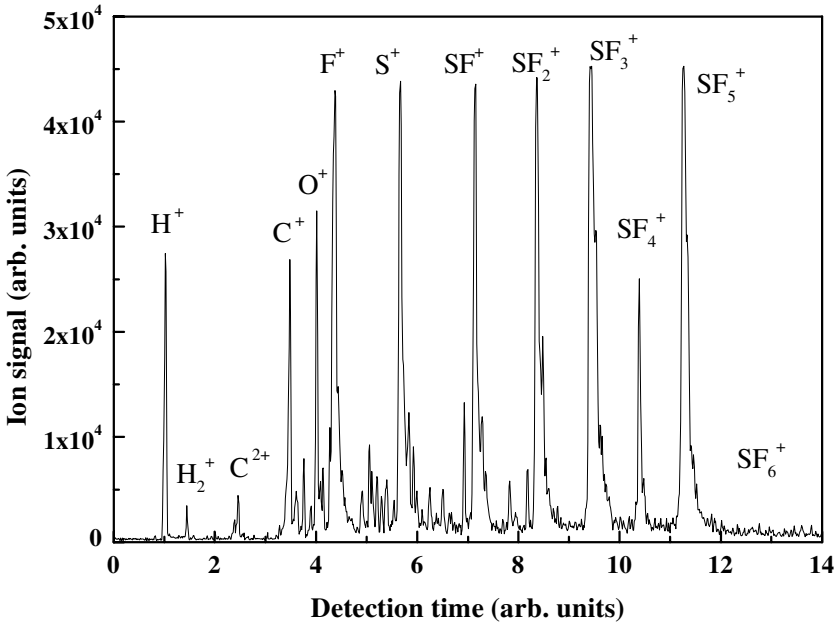

Figure 3.4 *Time-of-flight spectrum showing fragments of SF_6. No SF_6^+ was detected.*

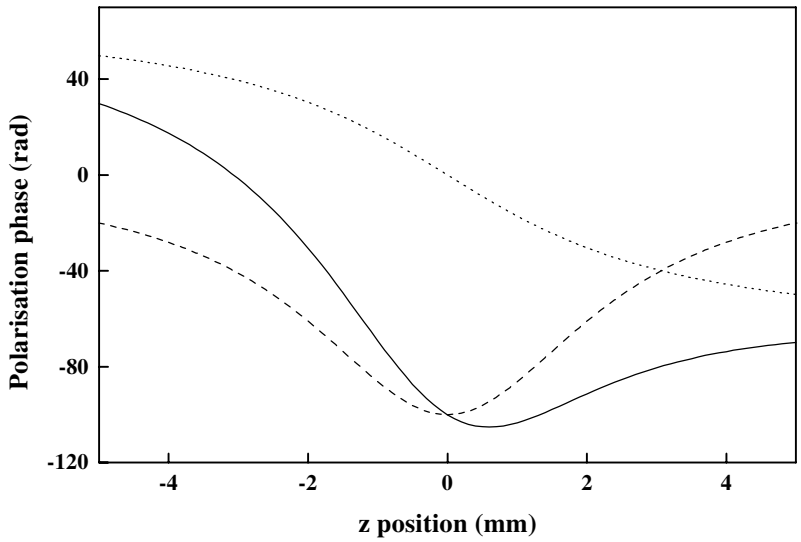

Figure 3.5 *The phase of the polarisation along the propagation axis (solid line). The phase due to the focusing is shown with a dotted line and the intensity dependent phase is shown with a dashed line.*

3.3 Macroscopic effects

3.3.1 Phase-matching

Harmonic generation is optimised when phase-matching is achieved, i.e. when the difference in phase between the induced polarisation and the generated field is minimised over the medium length. This allows an efficient energy transfer to the harmonic field. To characterise phase matching, one defines a coherence length, L_{coh}, as the length over which the generated field and the induced polarisation gets dephased by π.

There are essentially three contributions to the phase mismatch between the two fields. To begin with, **dispersion** makes different frequencies travel at different speeds and therefore get out of phase with each other. The main causes of dispersion (in a low-density gas jet) are the free electrons created by ionisation. Therefore, this effect is best avoided by keeping the intensity below the saturation intensity. Ionisation can play an important role in both the temporal and spatial profile of the harmonics. Secondly, there is the **Gouy phase shift** of π, that a laser beam experiences when going through a focus. This is shown by a dotted line in Figure 3.5. This leads to a phase variation of the polarisation equal to q times that of the fundamental. By using loose focusing and a short medium the phase shift within the medium is minimised. The third contribution to the phase mismatch is the **intensity dependence of the harmonic dipole phase**. Theoretical studies of high-order harmonic generation by a single atom exposed to an intense laser field

have shown that the dipole phase varies rapidly as a function of the laser intensity [34,35]. Obviously, if the phase depends on the laser intensity, it will be different for different atoms in the interaction volume, since the laser intensity varies strongly both in time and space in the medium. The dipole phase depends on the intensity, which for a Gaussian beam varies along the propagation axis as

$$I(z) = \frac{I_0}{1 + 4\,z^2/b^2} \tag{3.1}$$

where I_0 is the peak intensity, z is the coordinate along the propagation axis and b is the confocal parameter. The confocal parameter is defined as

$$b = \frac{2\pi\omega_0^2}{\lambda} \tag{3.2}$$

where ω_0 is the radius of the beam waist and λ the laser wavelength. The variation of the dipole phase is marked with a dashed line in the figure. The sum of the Gouy phase shift and the intensity-dependent phase shift is shown in Figure 3.5 with a solid line. In the region z<0 the slopes of the two phases add, leading to a rapid decrease of the total phase. However, when z>0 they have opposite signs and the total slope flattens out. Consequently, the optimal position for placing the medium should be after the laser focus. The phase shown in figure 3.5 is the phase of the polarisation *on axis*. For harmonic emission *off the propagation axis,* studies have shown that phase matching can be good even when the medium is placed before the focus [35]. This is the reason for the occurrence of annular harmonic beams when focusing after the gas jet. These effects have been studied extensively by Salières *et al.* [36] and will be discussed again in Chapter 4.

A promising method of achieving good phase-matching is to focus the laser into a gas-filled hollow-core fibre. This has recently been done by several groups [37-39] and high conversion efficiencies have been reported. Tamaki *et al.* [40] demonstrated harmonic generation also in a self-guided beam.

3.3.2 Focusing conditions

As discussed above, the focusing conditions strongly influence the phase matching. To make the solid slope in Figure 3.5 as flat as possible, loose focusing should be used. An important parameter for the focusing conditions is the confocal parameter, *b*, which has been defined in Equation 3.2 above. The confocal parameter is the distance over which the laser intensity is more than half the peak intensity. Experimentally, increasing the confocal parameter corresponds to using a long focal length lens or aperturing the beam. Using a long focal length means that the expansion of the beam is slower, something that should be taken into account when

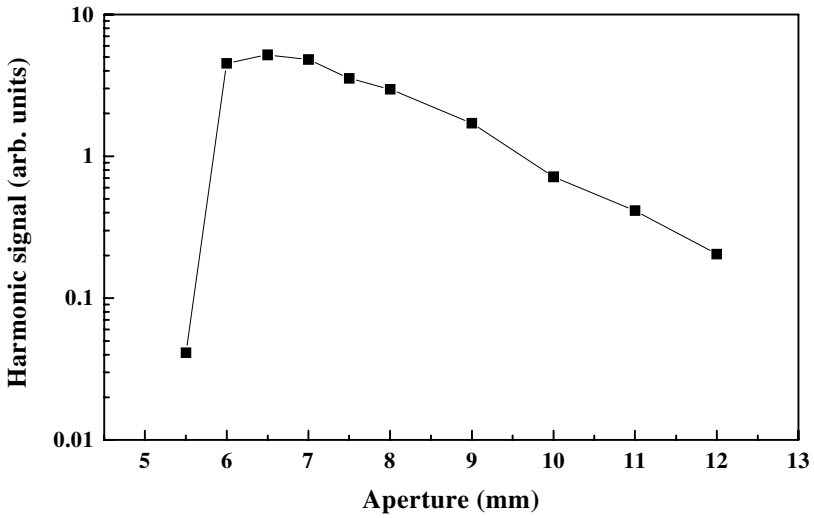

Figure 3.6 *The 21st harmonic as function of aperture. There is an optimal aperture where the harmonic signal has a maximum.*

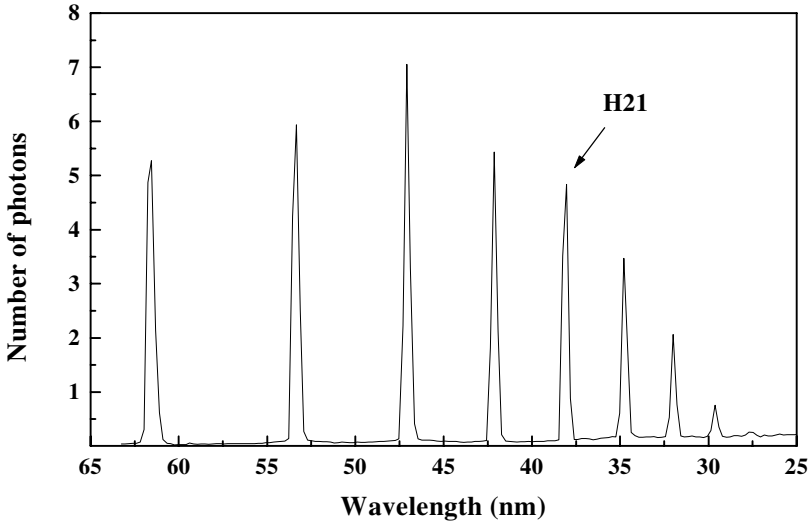

Figure 3.7 *Harmonic spectrum recorded with the optimal aperture for the 21st harmonic (6.5 mm) found in the previous figure. The experimental conditions are the same.*

considering the power density on the grating or on the spectrometer entrance slit, as discussed in connection with the experimental setup (Section 2.1). To illustrate the influence of focusing conditions, Figure 3.6 displays the strength of the 21st harmonic as function of the aperture, under certain experimental conditions. When closing the aperture the harmonic yield increases, despite a large part of the energy

in the beam being discarded. The harmonic yield increases partly because the phase variation of the polarisation on axis is decreased and partly because the harmonic-generating volume increases. Below a certain diameter the intensity in the focus becomes too low and there is a rapid decrease of the efficiency.

The harmonic spectrum recorded with an aperture of 6.5 mm (yielding the maximum signal for the 21st harmonic) is presented in Figure 3.7. The conditions are as for Figure 3.6. The optimal aperture places the 21st harmonic at the end of the plateau. This is where the compromise between intensity and long confocal parameter is optimised. Reducing the intensity further has a strong effect on the yield, once the harmonic becomes part of the cutoff.

3.3.3 Pressure effects

Harmonic generation is a coherent process and therefore, since the amplitudes of the fields emitted by the individual atoms are added together, the efficiency is expected to vary as the square of the atomic density. An easy way to increase the harmonic yield is therefore simply to increase the pressure. The pressure dependence has been studied by Altucci *et al.* [41] and indeed, they found a quadratic dependence on the pressure within a certain pressure range (between 3 and 80 mbar). Above this pressure the harmonic signal decreased. The decrease was attributed to the large density of free electrons created through ionisation. Most electrons are created where the intensity is the highest, i.e. in the centre of the beam. The free electrons give rise to a refractive index below one; this gradient will act as a negative lens defocusing the fundamental beam and thus decreasing the peak intensity. The pressure corresponding to the maximum emission decreases with harmonic order, exhibiting the stronger dependence of higher orders on laser intensity. The position of the cutoff moves towards lower harmonics when the gas pressure is increased. In the work in this thesis (Papers I-VIII), the gas pressure was normally kept relatively low, about 20 mbar, in order to minimise refraction and dispersion effects.

4. Temporal coherence of high-order harmonics

The difficulty in characterising harmonic radiation is reflected in the relatively few studies performed on the subject. Extremely short pulses and short wavelengths impose high demands on the detection equipment, often requiring elaborate experimental setups to be employed. The pulse length of high-order harmonics (21-27) has been measured by Bouhal *et al.* [42] and Glover *et al.* [43]. Both groups found the harmonic pulse length to be approximately 70% of the pulse length of the fundamental (which was 190 fs and 70 fs, respectively). The time evolution of lower order harmonics produced by picosecond lasers has been studied by Faldon *et al.* [44] and Starczewski *et al.* [45]. An overview of the spatial and spectral characteristics is given by Salières *et al.* [36]. The spatial profile has been investigated in [46-49] and the spatial coherence in [36,50]. In Paper III we present the first measurements of the temporal coherence of high-order harmonics.

Our interest in the temporal coherence of harmonic radiation is two-fold. Firstly, one gains insight into the dynamics of an atom exposed to a strong laser field and a possibility to test theoretical models. Secondly, the temporal coherence is in some sense a measure of the 'quality' of the harmonic radiation, since it is directly related to the bandwidth. Narrow bandwidth radiation is hard to achieve and is important in the applications discussed in Papers VI, VII and VIII. For some applications, the most obvious one being XUV interferometry, good temporal coherence is of interest.

In Papers II, III and IV we report on experiments investigating properties related to the temporal coherence of harmonic radiation. We start in Paper II by demonstrating that two harmonic sources generated independently in a gas jet by the same laser are locked in phase. Once this is established we proceed to measure the temporal coherence of the harmonic radiation and investigate the parameters determining the temporal coherence. Paper III describes the first findings of these studies. In Paper IV a more systematic study and a more extensive theoretical interpretation are made. We use the results of these studies to perform XUV interferometry, which is discussed in Section 5.2 and Paper V.

4.1 Definition of temporal coherence

The temporal coherence can be defined as *'the time over which an electro-magnetic field maintains a near constant phase relationship'*. This is traditionally what is measured in a Michelson interferometer; the field is split into two identical fields and one of them is delayed by translating a mirror. The interference pattern, formed when the two pulses are superimposed in space, is recorded. The degradation of contrast in the interference pattern as the delay is increased is a measure of the degree of coherence.

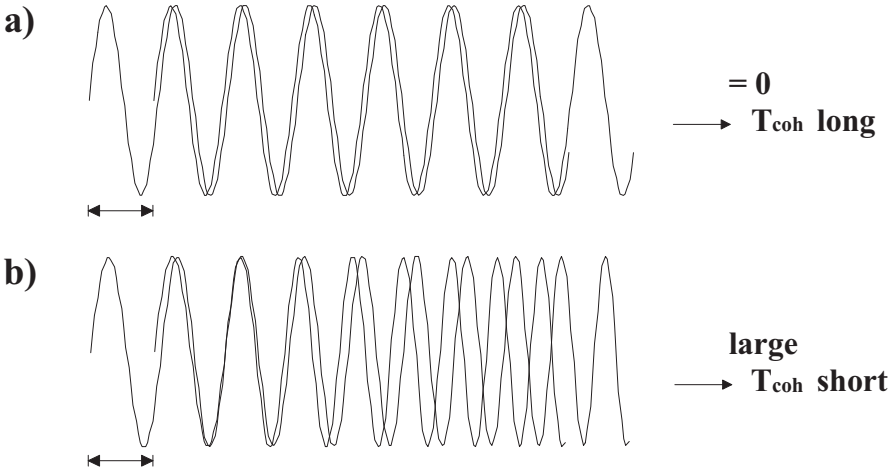

Figure 4.1 *An illustration of the relationship between bandwidth and temporal coherence. A long temporal coherence corresponds to a small bandwidth, and vice versa.*

Figure 4.1 illustrates the relationship between temporal coherence, T_{coh}, and bandwidth, $\Delta\omega$. In Figure 4.1a the field is monochromatic. As the pulse is delayed by the time, τ, the phase relationship stays constant. On the other hand, in Figure 4.1b, the pulse is chirped and therefore has a larger bandwidth. When one pulse is delayed relative to the other, the phase relationship changes and the interference fringes are smeared out. The temporal coherence is inversely proportional to the bandwidth [51],

$$T_{coh} \propto \frac{1}{\Delta\omega} \tag{4.1}$$

4.2 Theoretical predictions

Since the phase depends on the laser intensity, it will be time dependent due to the variation of intensity during the laser pulse. This will then lead to a frequency chirp of the generated harmonic radiation and a decrease of the temporal coherence. According to [34] the phase of the harmonic dipole is proportional to the intensity of the driving field

$$\phi(r,t) = -\alpha\, I(r,t) \tag{4.2}$$

The constant of proportionality, α, is closely related to the excursion time, τ, in that the *variation* of α follows the *variation* of τ. The excursion time is the time the

electron spends in the continuum, as described in the semi-classical model. This means that a longer excursion time corresponds to a larger α. The relationship between α and τ allows us to relate spectral properties of the emitted harmonics to the dynamics of the electron in the continuum. We shall return to this in Section 4.5.

4.3 Experimental setup

The configuration that the experiment is based on, along with some relevant notation, is presented in Figure 4.2. Two harmonic sources, separated by a small distance, δ, are created in two foci in the gas jet. The far-field interference pattern of the harmonic radiation, of wavelength λ, is observed at a distance L from the source. The instantaneous fringe pattern, at a point y in the observation plane, is given by the following expression

$$I(t) = I_1(t) + I_2(t) + 2\sqrt{I_1(t)I_2(t)} \times \cos\left[2\pi \frac{\delta y}{\lambda L} + \phi_1(t) + \phi_2(t)\right] \qquad (4.3)$$

where $\phi_1(t)$ and $\phi_2(t)$ are the dipole phase terms that are dependent on the laser intensity. The interference pattern observed in the far field is obtained by integrating *I(t)* in time over the entire pulse. If $\phi_1(t) - \phi_2(t)$ varies by more than π during the harmonic pulse the fringe pattern will be smeared out. The contrast, or visibility, *V*, of the fringes is defined as

$$V = \frac{(I_{\max} - I_{\min})}{(I_{\max} + I_{\min})} \qquad (4.4)$$

From Equation 4.3 can be seen that there are two time-dependent parameters that affect the visibility of the fringes, the intensity ratio of the two fields and the phase variation of the two fields.

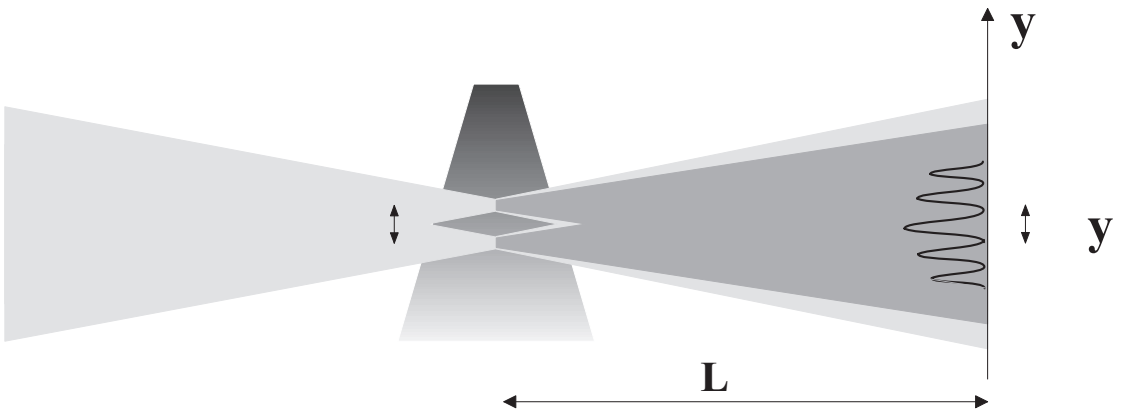

Figure 4.2 *The setup used to create two spatially separated harmonic sources.*

A layout of the setup is shown in Figure 4.3, employing two different ways of creating two separate harmonic sources. In **Setup 1** (described further in Paper II) the beam is separated into two spatially displaced parallel beams of orthogonal polarisation using a birefringent crystal with the axes oriented at 45° to the laser polarisation. The polariser placed after the crystal transmits a common polarisation component of the two beams. The intensity ratio in the two beams can be varied continuously by rotating the polariser. The crystal introduces a time delay between the two beams, due to the different refractive indices. However, this time delay is negligible compared to the pulse duration of 35 ps. In **Setup 2** (used for the experiments described in Papers III and IV) the time delay between the two pulses can be varied, allowing measurement of the temporal coherence. Shorter laser pulses (100-110 fs) were used to produce higher intensity, thus imposing a more stringent test on the effect of the intensity-dependent dipole phases. A Michelson interferometer splits the laser pulse into two identical pulses with a variable time delay between them. The time delay is controlled by manually translating one pair of mirrors. One mirror is slightly tilted so that the two beams are not completely parallel and therefore focused into two slightly different positions. Hence, we produce two sources of harmonics at a close distance but spatially separated.

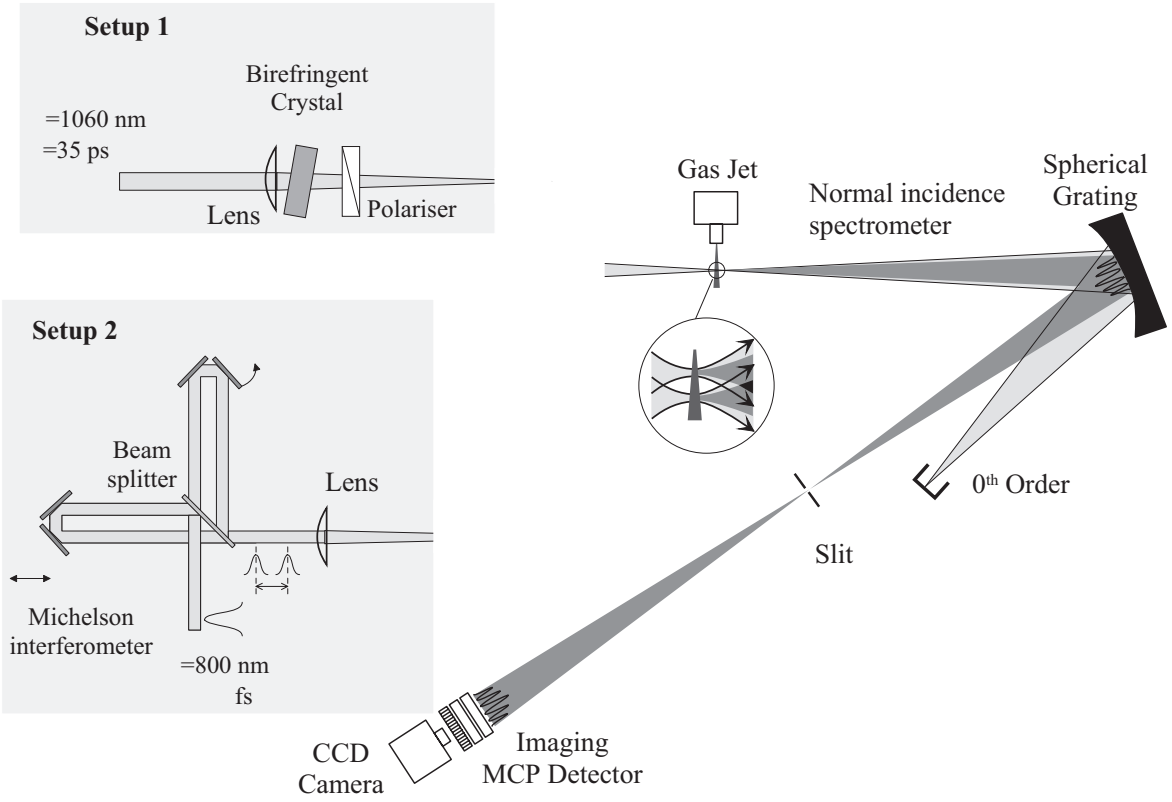

Figure 4.3 *Experimental setup showing two ways to generate two spatially separated harmonic sources.*

The harmonic beams from the two sources are practically superposed in the far field, giving rise to an interference pattern. A grating is used to select a given harmonic order and project it on to a micro channel plate (MCP), coupled to a phosphor screen. The image on the phosphor screen is captured with a CCD camera.

The experiment described in Paper III was performed at LENS (European Laboratory for Non Linear Spectroscopy) in Florence, Italy, with a 100 fs Ti:sapphire laser giving 0.7 mJ/pulse. This allowed us to see interference fringes in harmonics up to the 21st. Paper IV describes more systematic studies performed in Lund using the Ti:sapphire laser giving pulses of 110 fs. Orders up to the 31st could then be produced with enough photons for fringes to be visible.

4.4 Experimental results

Using Setup 1 we obtained interference fringes from the 7th to the 17th harmonic generated in xenon. The position of the fringes was stable on a shot-to-shot basis with a visibility around 30%. The origin of this low visibility is not quite clear; one possible reason can be ionisation of the medium, leading to a blueshift of the fundamental and, as a result, a blueshift of the harmonics. Fringes were observed with a decreasing contrast as the intensity difference in the two foci was increased. However, with an intensity ratio of 0.6 a visibility of 6% was still observed. This might seem surprising considering the predictions of the intensity-dependent phases. Only if the intensities in the two beams are exactly the same, are the emitted harmonics expected to have a constant phase relationship. To interpret these results we performed numerical simulations for conditions similar to the experimental ones. We found that we could reproduce the experimental results very well. In the simulations the influence of the intensity-dependent phase variation could be 'turned on or off', and very little difference was seen between the two results. The intensity-dependent phase variation was simply not large enough to introduce a significant chirp of the harmonic fields. To thoroughly test the theoretical models predicting an intensity-dependent phase variation the experiment should be performed at higher intensities.

Using Setup 2 the required higher intensities could be delivered in the same two-foci configuration, with the added possibility of varying the time delay between the two pulses. In Figure 4.4 interference patterns for harmonic orders from the 7th to the 21st, created in argon, are presented when the two pulses are superposed in time. The fringe separation (Δy) decreases with increasing harmonic order, due to the shorter wavelength according to

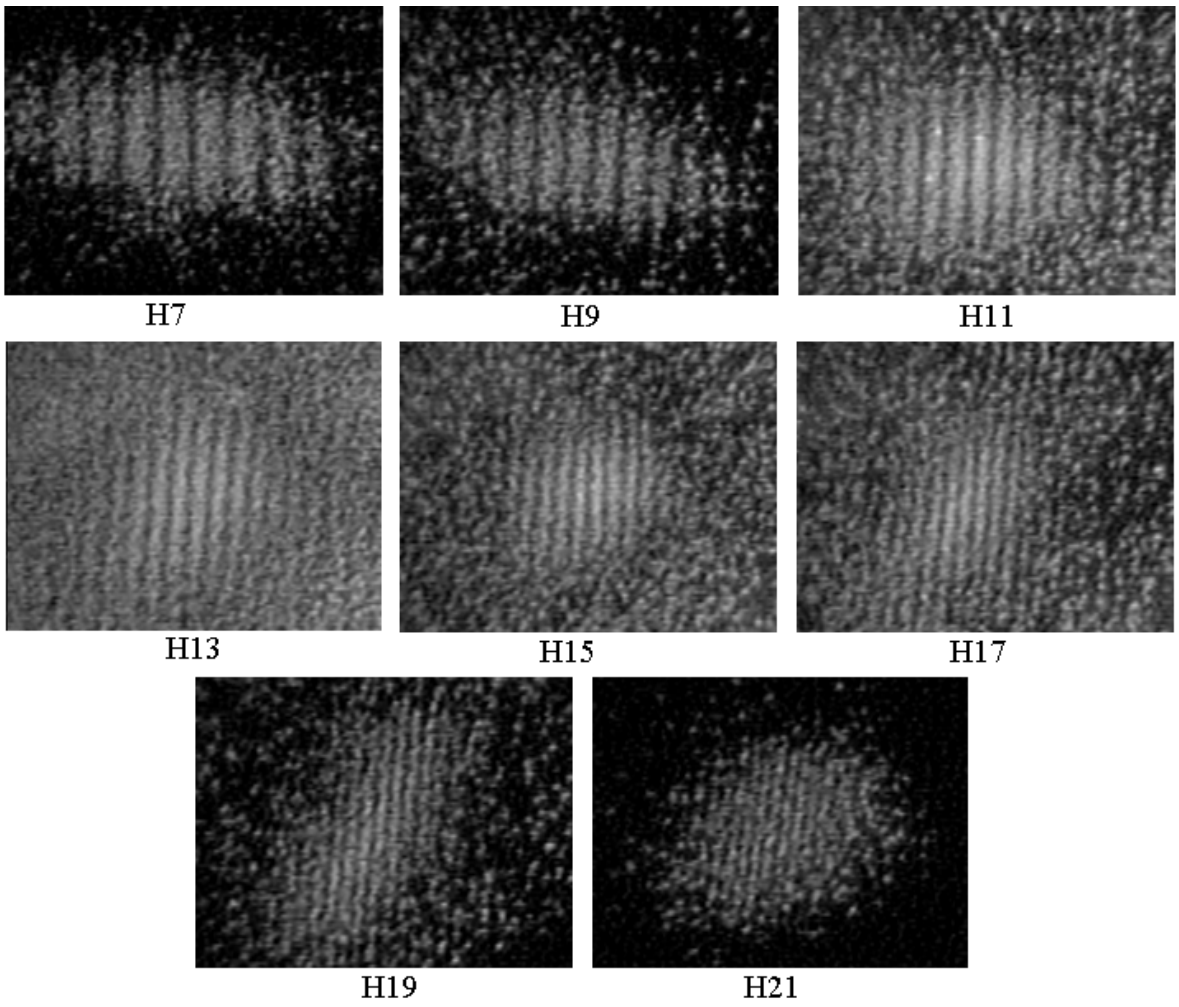

Figure 4.4 *Interference fringes for the 7th to the 21st harmonic generated in argon. The two beams are superposed in time.*

$$\Delta y = \frac{\lambda L}{\delta} \tag{4.5}$$

For some harmonics, in certain focusing conditions, we found two different regions in the harmonic profile with different coherence times. Figure 4.5 shows the far-field pattern of the 13th harmonic for two different time delays, τ, between the pulses 0 fs (a) and 25 fs (b). Two distinct spatial regions can be seen, an inner intense region and an outer less intense region. Fringes exist in both regions in (a) while the fringes in the outer region have disappeared in (b), demonstrating that the coherence time in the inner region is longer than in the outer. To understand these

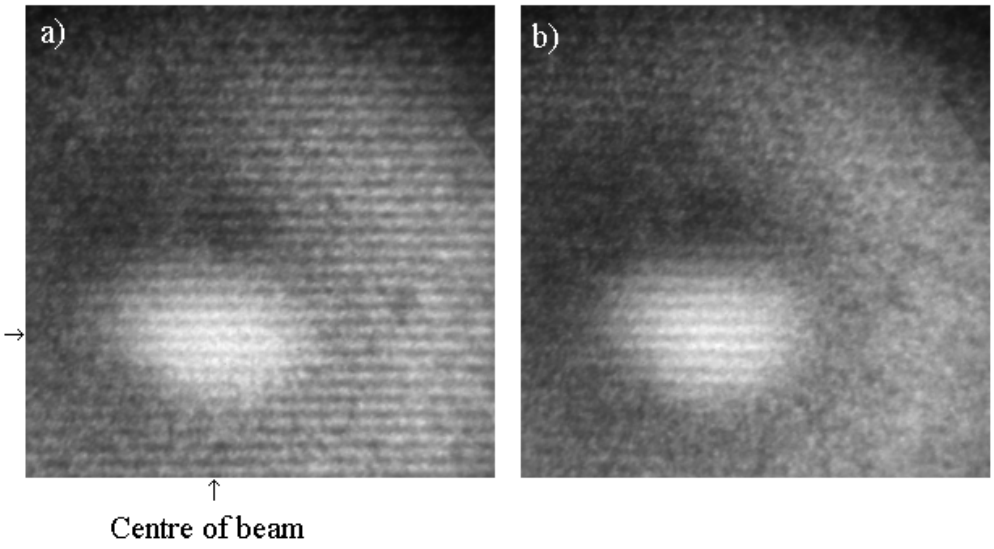

Figure 4.5 *Interference fringes for the 13th harmonic generated in argon. In a) the two beams are superposed in time, whereas in b) one beam is delayed by 25 fs.*

results we made a systematic study of how the coherence times in the two regions vary as a function of harmonic order, intensity and focusing conditions.

Figure 4.6a shows the dependence on harmonic order for a constant intensity of 4×10^{14} W/cm^2, and in (b) the dependence of the 23rd harmonic on intensity is presented. A different behaviour is observed for the two regions; the coherence time for the outer region (open circles) is short and approximately constant with respect to harmonic order and intensity, whereas the coherence time for the inner region (solid diamonds) decreases with harmonic order and increases with intensity. In both cases the two regions merge in the cutoff. An increase of the intensity corresponds to moving harmonics in the plateau region away from the cutoff. From these results we therefore conclude that as the harmonic is moved away from the cutoff the coherence time of the inner region increases, whereas the outer region is relatively insensitive. It should be noted that the coherence time in the inner region is very long. Considering that the fundamental pulse length is 110 fs, and that the harmonic pulse length is shorter than the fundamental [42,43], the coherence time is comparable to the harmonic pulse length.

The influence of the focusing position relative to the gas jet was studied and is discussed in detail in Paper IV. The laser focus was placed before, after and in the gas jet, and in each position the coherence times of the two regions were measured. To summarise the results, we found that the coherence times in the two regions were approximately constant, independently of the position relative to the gas jet. However, the phase-matching conditions affected the two regions differently; the outer region in particular was sensitive to the position of the focus relative to the gas jet.

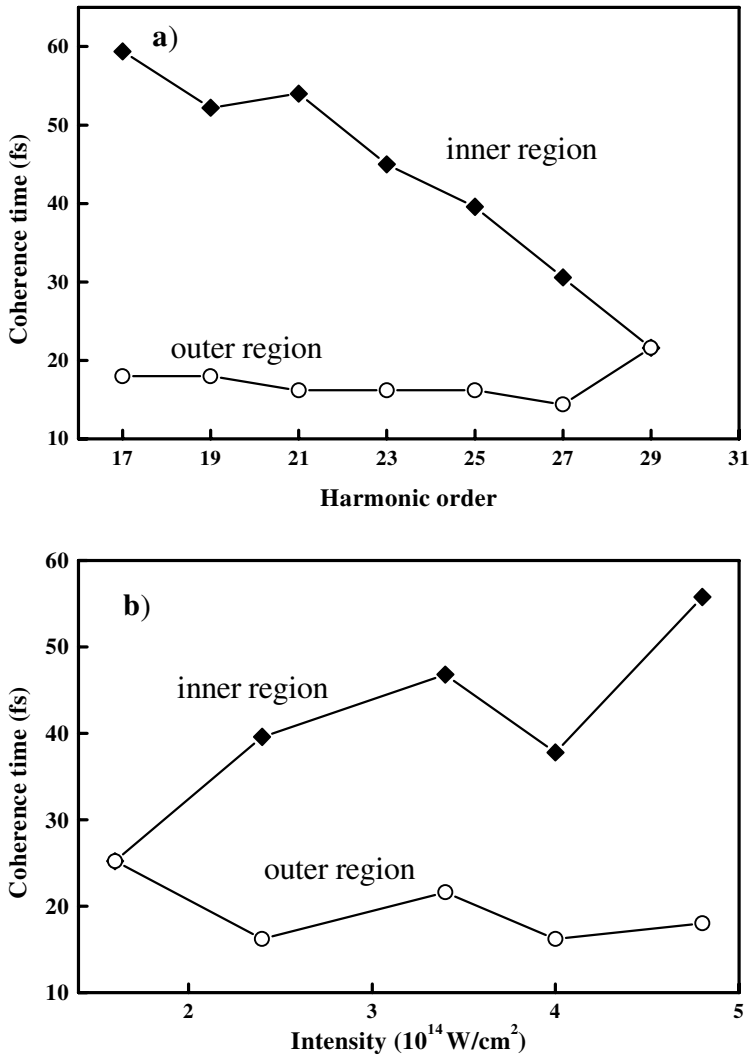

Figure 4.6 *Coherence times as a function of a) harmonic order and b) laser intensity. The inner region is marked with solid symbols and the outer with open symbols. The two regions merge in the cutoff region.*

4.5 Theoretical models

Below, theoretical models of harmonic generation are presented. We begin by discussing a simple classical model; the detail with which it is treated is motivated by the fact that it gives a very intuitive explanation of the results presented in this chapter. Numerical simulations that have been performed in conditions similar to the experiment are also discussed.

4.5.1 Classical interpretation

To understand the experimental results we return to the semi-classical model and study the process where the electron is accelerated classically by the laser field. We make a simple model by neglecting the influence of the atomic core and consider only the motion of a free electron in a laser field. The field is treated as having a slowly varying amplitude, so that the peak electromagnetic field (E_0) can be treated as constant during a single optical cycle. The force the electron experiences is proportional to the laser field $E=E_0 sin(\omega t)$. Assuming the electron to have zero velocity immediately after tunnelling ionisation, at position $x=0$ at time $t=t_0$, we solve the classical equations of motion, and express the dynamics of the electron according to

$$v(t,t_0) = -v_0 \cos(\omega t) + v_0 \cos(\omega t_0) \tag{4.6}$$

$$x(t,t_0) = \frac{1}{\omega}(-v_0 \sin(\omega t) + v_0 \sin(\omega t_0)) + (t-t_0)v_0 \cos(\omega t_0) \tag{4.7}$$

where $v_0=qE_0/m\omega$. Depending on the phase of the electric field at the release time the electron will follow different trajectories in the continuum. Figure 4.7 displays different electron trajectories depending on when in the laser cycle the electron is ionised. The laser field is marked with a dotted line. Electrons ionised in the first quarter of the cycle, while the field is growing, are driven away from the atom and do not return to it (dashed lines). These electrons will not contribute to harmonic generation. Electrons released between T/4 and T/2 will pass the core again, and

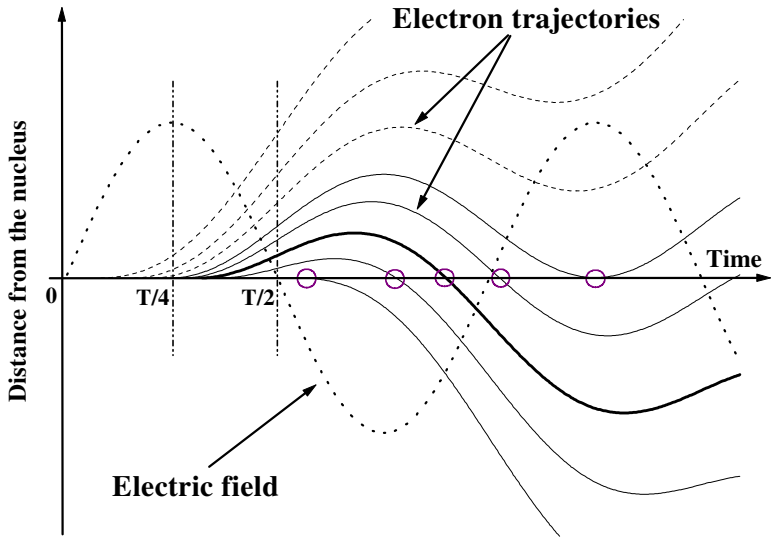

Figure 4.7 *Different electron trajectories in the continuum corresponding to different release times. The return kinetic energy is given by the slope when the trajectory crosses the time axis.*

have a certain probability of recombining. The kinetic energy upon return determines the harmonic order emitted (high kinetic energy in Figure 4.7, corresponds to a large slope when crossing the time axis). The trajectory with the highest kinetic energy, corresponding to the cutoff harmonic, is drawn with a thick line. On both sides of the trajectory with maximum kinetic return energy, there are trajectories returning to the nucleus with less energy. This means that for all energies less than the maximum return energy, there will be two different trajectories. We neglect the trajectories with an excursion time longer than one optical period since their influence is small. A different presentation of the trajectories is given in Figure 4.8 where the return energy is plotted as a function of release time (solid line). The time spent in the continuum (the excursion time, τ) is plotted in the same figure with a dashed line. The maximum return energy the electron can have when it returns to the core (3.2 U_p) corresponds to a release time of approximately 0.3T (107°). Harmonics in the plateau (from electrons with kinetic energy less than 3.2 U_p) are essentially generated by two different classes of electrons, with two different release times and, correspondingly, different amounts of time spent in the continuum. The difference in excursion time increases as the harmonic is moved further away from the cutoff.

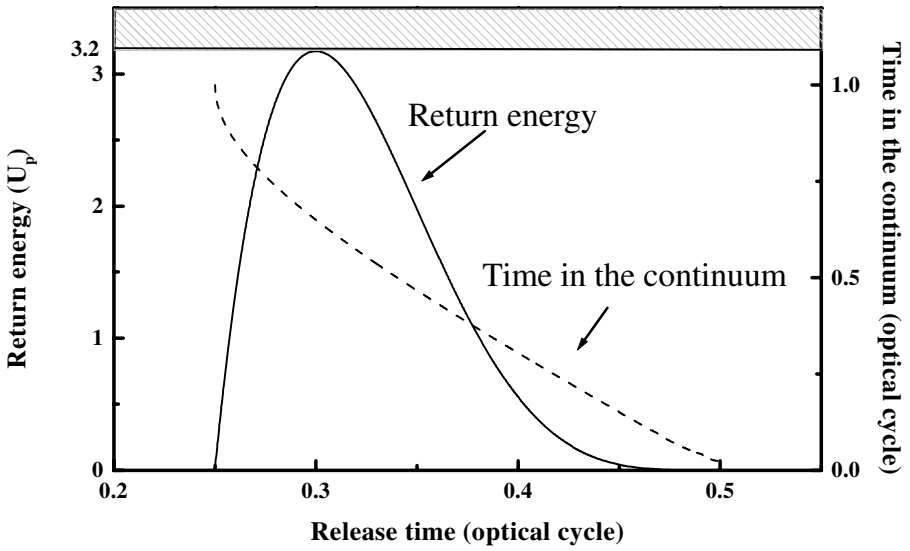

Figure 4.8 *Return kinetic energy (solid line) and excursion time (dashed line) as a function of the release time.*

Recalling Equation 4.2, we know that the phase depends on the intensity with the proportionality factor α. As mentioned above, a longer excursion time corresponds to a larger α. Consequently, the dipole phase can be related to the excursion time. In the plateau there are two different excursion times for each harmonic. Correspondingly, there are two different phase dependencies on the intensity. The intensity varies over the pulse both temporally and spatially *I(r,z,t)*. The **temporal variation**, *I(t)*, will produce a chirp in the emitted field corresponding to a spectral broadening; and through that a decrease of temporal coherence. The **radial variation**, *I(r)*, will affect the curvature of the phase front of the harmonics, thus determining the divergence of the emitted beam. From this follows that the short trajectory, τ_1, corresponding to a small α_1, will be associated with a long temporal coherence and a small divergence. These are precisely the properties of the inner region in Figure 4.5. On the other hand, the long trajectory, τ_2, with a large α_2, is associated with a short temporal coherence and a large divergence. This corresponds to the outer region in Figure 4.5.

Keeping in mind that the inverse of the excursion time is related to the temporal coherence we plot the inverse of the two classical return times, $1/\tau_1$ and $1/\tau_2$, to display the variation of the coherence time with harmonic order (Figure 4.9). The figure illustrates how the two curves merge when the photon energy increases, becoming identical at the cutoff. The features in this figure are very similar to our experimental results (Figure 4.6a) demonstrating that, despite the simplicity of this model, it can qualitatively explain our results.

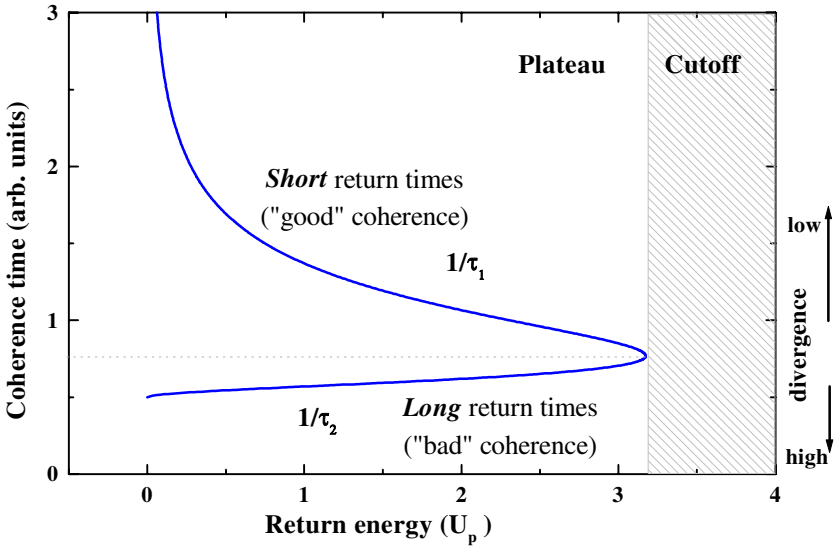

Figure 4.9 *Relative coherence times showing the two branches due to the two different trajectories, τ_1 and τ_2. At the cutoff the two branches merge.*

Since the different trajectories have different phase responses they are phase-matched differently. The independence of the coherence times on the focus position indicates that the temporal coherence is essentially determined by the single-atom dynamics, and not by propagation effects.

Returning to Figure 4.4, it can be seen that the 7th and 9th harmonics both display only one region. In harmonics 11 to 17 two regions can be seen and the divergence of the harmonic beam is larger. Harmonics 19 to 21 belong to the cutoff where the two regions merge and the photon yield is lower. Using 800 nm laser light *($h\nu$=1.56 eV)*, the 11th harmonic is the first harmonic with a photon energy above the ionisation potential of argon *(I_p=15.8 eV)*. From the figure we see a difference in behaviour between the harmonics $h\nu_q<I_p$ and $h\nu_q>I_p$. The harmonics $h\nu_q<I_p$ are probably better described by a multiphoton picture than by the semi-classical model and consequently might not present the same intensity-dependence of the phase.

4.5.2 Numerical simulations

Numerical simulations of high-harmonic generation involve two steps: the calculation of the single-atom emission spectrum and, subsequently, the propagation of the generated harmonic field in the nonlinear medium. The calculation of the emission from a single atom can be done using several different approaches. The semi-classical model mixes classical and quantum mechanical processes: the tunnelling and recombination of the electron is described by quantum mechanics, whereas the motion of the electron in the field is treated classically. A fully quantum mechanical description of the semi-classical model was formulated by Lewenstein *et al.* [52] with the **strong field approximation (SFA)**. Here important quantum mechanical effects like quantum diffusion and quantum interferences are included. Three main assumptions are made:

- Only the ground state of the atom is considered, all other bound states are neglected
- Depletion of the ground state is neglected
- The liberated electron is treated as a free particle in the laser field with no effect of the Coulomb potential

These approximations are only valid when there are no intermediate resonances and the Keldysh parameter ($\gamma = \sqrt{I_p / 2U_p}$) is less than one (i.e. in the tunnelling regime). The SFA predicts the existence of two dominating electron trajectories for the plateau harmonics [34] and provides an intuitive model. It is a relatively simple model that can reproduce many experimental results. However, it is mainly valid for high-order harmonics and often underestimates the harmonic strengths.

A more accurate description of the dynamics of the atom-laser interaction is obtained by direct numerical integration of the **time-dependent Schrödinger equation (TDSE)** within the single active electron approximation (SAE). This procedure is described in detail by Kulander *et al.* [53]. In the SAE the orbitals are frozen for all electrons except one, the single active electron.

Once the single atom data is obtained, a complete calculation is performed including propagation through the medium, where effects of phase matching are taken into account. This method has been described in [54,55]. The single-atom response is used as input data in the numerical calculations performed to calculate the response of the macroscopic system. This involves solving Maxwell's equations for both the harmonic and the fundamental field, using the slowly varying envelope approximation and the paraxial approximation.

We performed a complete calculation, including both single atom and propagation effects, in conditions similar to those in the experiment. Intensity-dependent single atom data were obtained by solving the TDSE and subsequently performing an adiabatic approximation [54,56], and were used as a source term in the propagation calculations. Although there is some difference in absolute values, the resulting coherence times show good agreement with our experimental results (see Paper IV). Gaarde *et al.* [57] have made further numerical simulations based on both the SFA and the TDSE, reproducing nicely the results from Paper III. In particular the far-field interference pattern of the 15^{th} harmonic in argon is analysed spectrally and spatially, producing results in good agreement with the experimental results.

5. Applications of high-order harmonics

Since its first discovery high-harmonic generation has been recognised as a promising source of coherent short-wavelength radiation. The field has now matured and some laboratories are starting to use harmonic radiation for applications rather than to study the underlying physics behind the process itself. Haight and Peale [58] studied the ultra-fast dynamics of electrons at solid surfaces by using the 5^{th} to the 11^{th} harmonic of a 610 nm laser. Plasma diagnostics were performed by Theobald *et al.* [59], where the electron density was determined by measuring the transmittance of different harmonics. A number of spectroscopic applications have been performed in Lund on different atoms and molecules; He [60,61, Paper VIII], CO [Paper VII] and NO [62]. Recently, the possibility of high temporal resolution, in the femtosecond regime, has been utilised in an experiment where the time evolution of excited molecular states has been studied in acetylene [63].

This thesis deals with three different applications of harmonic radiation. The first two are spectroscopic studies of CO (Paper VII) and He (Paper VIII), where the tunability and narrow bandwidth of harmonic radiation are essential. These experiments are performed using the Lund XUV system (a tunable picosecond laser followed by high-harmonic generation). The third application is XUV interferometry (Paper V), where the femtosecond system is used in order to gain temporal resolution. Paper IX and X concern lifetime measurements in Ge and Zr, respectively. These papers have been placed in an appendix since the measurements have not been performed using high-harmonic generation.

This chapter starts with a summary of the spectroscopic measurements presented in Papers VII, VIII, IX and X and an overview of the XUV system. Following this, XUV interferometry using harmonic radiation is described. This is presented further in Paper V.

5.1 Spectroscopy using narrow-bandwidth harmonic radiation

Spectroscopy is used for the mapping of the energy-level structure of an atomic or molecular system. The spectrum is formed by the emission or absorption of electromagnetic radiation as the atom or molecule changes its electronic configuration.

Measurements of lifetimes of excited states of atoms and molecules are of great interest both from a theoretical point-of-view and where applications are concerned. Lifetimes of excited states are useful for theorists to model the structures of atoms and molecules. The transition probability, which represents the probability that an atom in a certain state will, through radiative decay or absorption, transfer to another state, is directly related to the radiative lifetime. The

transition probability is well suited to test the validity of calculated wave functions. The calculated transition probability is very sensitive to errors made in the approximations (more than the calculated energy levels) and a comparison between calculated values and those deduced from experimentally measured lifetimes is therefore a sensitive indicator of these errors. In Paper VIII we measure photo-ionisation cross-sections of excited states in helium and compare them with theoretical values.

Transition probabilities are of great importance in plasma physics and astrophysics. Accurate transition probabilities are necessary for the analysis of stellar spectra in astrophysics, where spectral lines are the main source of information. Errors in the transition probabilities will directly propagate into the determination of the abundance of different elements. Many important transitions in the UV/VUV cannot be seen from earthbound telescopes due to absorption in the atmosphere. The launch of the Hubble Space Telescope opened up new spectral regions for observations and the importance of obtaining accurate spectroscopic data in those regions has increased substantially. Papers VII, IX and X report on lifetime measurements of astrophysical interest.

5.1.1 Theoretical background

The probability that an excited state, *i*, will decay into a lower state, *k,* is given by the Einstein coefficient A_{ik},

$$A_{ik} = \frac{8\pi^2}{3}\frac{\nu^3}{\varepsilon_0 \hbar c^3}\left|\left\langle \psi_k \left| e\bar{r} \right| \psi_i \right\rangle\right|^2 \qquad (5.1)$$

The dipole operator is given by $e\bar{r}$ and the wavefunction of the upper and lower state by ψ_i and ψ_k, respectively. The total probability for spontaneous transitions from one state is achieved by summing over all possible lower levels that the atom can decay to

$$A_i = \sum_k A_{ik} \qquad (5.2)$$

The average time an atom spends in an excited state is given by the lifetime, τ_i, which is related to the transition probability by

$$\tau_i = \frac{1}{A_i} \qquad (5.3)$$

The population density in the excited state, N_i, will decrease exponentially with time

$$N_i = N_{i0} e^{-t/\tau_i} \tag{5.4}$$

where N_{i0} is the population density at $t=0$. Usually several possible decay channels exist. The branching ratio (BR) is a measurement of what part of the total decay will go through a particular channel. To determine the transition probability between two states from a lifetime measurement a knowledge of the branching ratio is required

$$BR = \frac{A_{ik}}{\sum_k A_{ik}} \tag{5.5}$$

If only one decay channel exists or if other channels are negligible, the transition probability can be determined directly from the lifetime. The oscillator strength, f_{ki}, is directly related to the transition probability and is given by:

$$f_{ki} = \frac{g_k}{g_i} \frac{2\pi\varepsilon_0 mc^3}{\omega_{ik}^2 e^2} A_{ik} \tag{5.6}$$

where g_k and g_i are the statistical weights of the two states. The oscillator strengths are used when modelling the observed spectra from objects of astrophysical interest. The abundance of different elements can be determined if knowledge of the corresponding oscillator strengths exists.

5.1.2 Description of the XUV system

In many spectroscopic applications both a high spectral and a good temporal resolution are desired. However, this is in conflict with the Heisenberg uncertainty relationship and a compromise has to be made. When a laser is used to selective populate an excited state, the bandwidth of the light should ideally match the Doppler width of the spectral line, to make efficient use of the photons. The use of high-harmonic generation to reach wavelengths in the XUV requires a relatively high power. This, together with the requirement of a relatively good temporal resolution makes a pulse length in the picosecond region suitable for the spectroscopic applications discussed in this thesis. The simultaneous requirements of tunability, short pulse length, narrow bandwidth and high intensity requires an advanced laser setup. The XUV system at the Lund High-Power Laser Facility is designed to meet these requirements. A layout of the system is shown in Figure 5.1 and the individual components are described briefly below. A more extensive description is given in Paper VI.

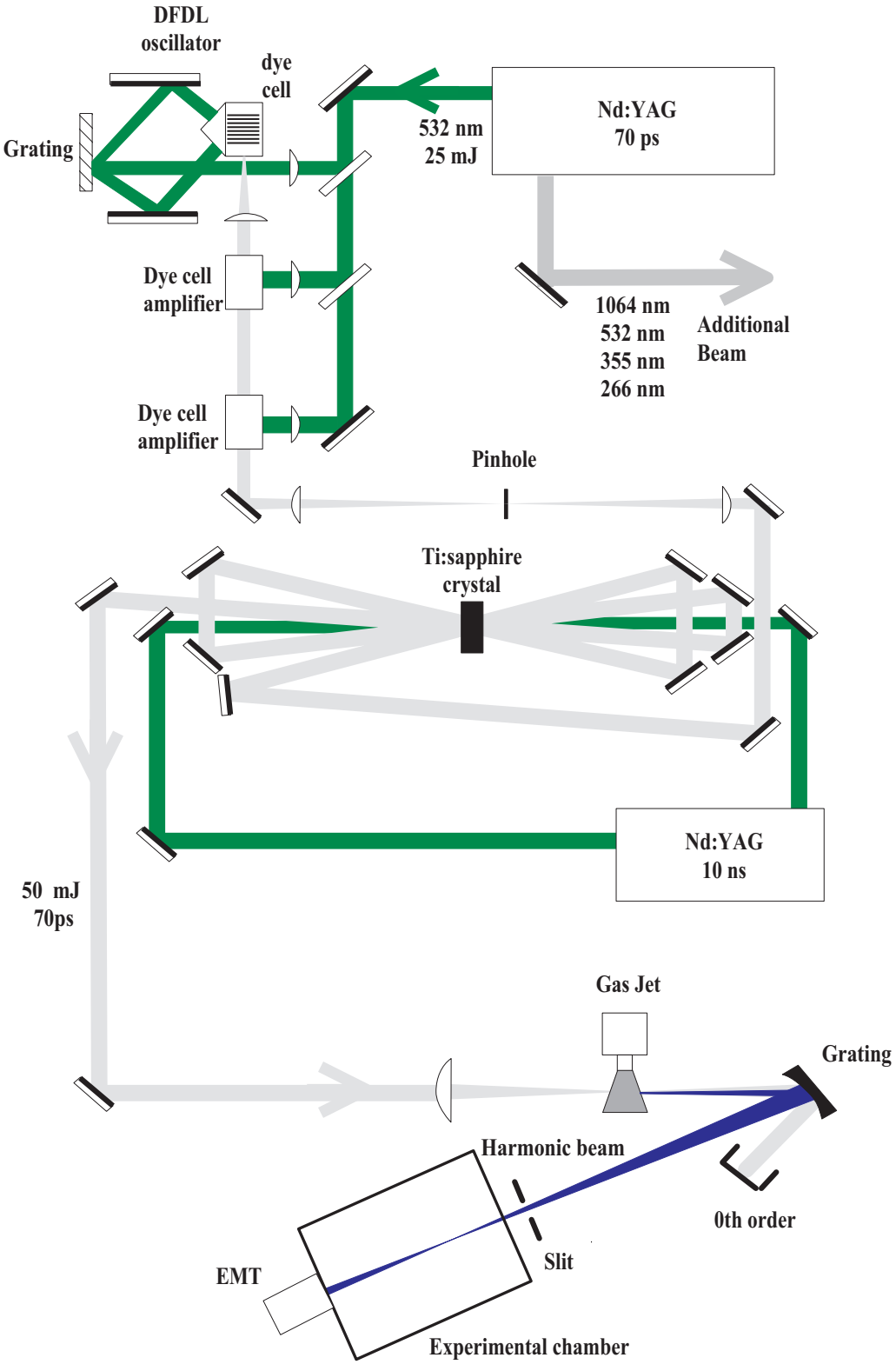

Figure 5.1 *Layout of the Lund XUV system.*

The pulse originates in a **Q-switched, mode locked, picosecond Nd:YAG laser**, operating at 10 Hz. The oscillator can be operated in two different modes, depending on how the mode locking and Q-switching is done, giving pulses of approximately 35 ps or 70-80 ps. The latter mode is used when the laser is used as a pump laser in the XUV system, due to the reduced trig jitter in this mode. This allows synchronisation with a second pump laser which is part of the final amplification stage.

To create tunable radiation with a narrow bandwidth we use a **distributed feedback dye laser (DFDL)**. Details about the oscillator can be found in [64,65, Paper VI]. The DFDL is pumped with the frequency doubled output from the Nd:YAG laser. A part of the pump beam is separated with a beam splitter, is focused with a cylindrical lens and diffracted by a grating into the $+1^{st}$ and -1^{st} orders. The two beams are spatially overlapped in a dye cell and an interference pattern is formed, where the period is determined by the angle between the pump beams. This periodic structure will act as a Bragg grating where the emission at a wavelength (λ_{DFDL}) corresponding to half the period of the Bragg grating will interfere constructively according to:

$$\lambda_{DFDL} = \frac{n_s \lambda_p}{\sin\theta} \tag{5.7}$$

Here λ_p is the wavelength of the pump laser, n_s is the refractive index of the solvent and θ is the angle between the incident laser beams and the normal of the dye cell. Tuning of the laser is either done by changing the refractive index of the solvent (by changing the temperature) or by changing the angle θ (by turning the mirrors). The limit of the tuning range is set by the emission of the dye in use.

The output from the oscillator is amplified in two dye amplification stages pumped by the remaining part of the pump beam. After this amplification an output of up to 5 mJ is obtained, which is enough for many applications, but does not allow for high-harmonic generation. When the DFDL is operated in the wavelength region between 700 and 900 nm it is possible to amplify the output in a Ti:sapphire crystal pumped by a nanosecond Nd:YAG laser. After the amplification stage an energy of up to 70 mJ is achieved. To avoid damaging the optics the system is usually operated with the maximum pulse energy limited to 50 mJ. The beam is focused with a lens with a focal length between 15 and 25 cm. Selection of the appropriate harmonic is done with a normal incidence grating, which also refocuses the beam into an experimental chamber where the experiment is performed.

By choosing the appropriate dye in the DFDL, and generating harmonic radiation either with the fundamental from the DFDL, or the frequency doubled beam, the whole spectral range from 180 nm down to approximately 35 nm can be covered. Typical harmonic spectra are shown in Figure 5.2. In (a) the DFDL is tuned to 760

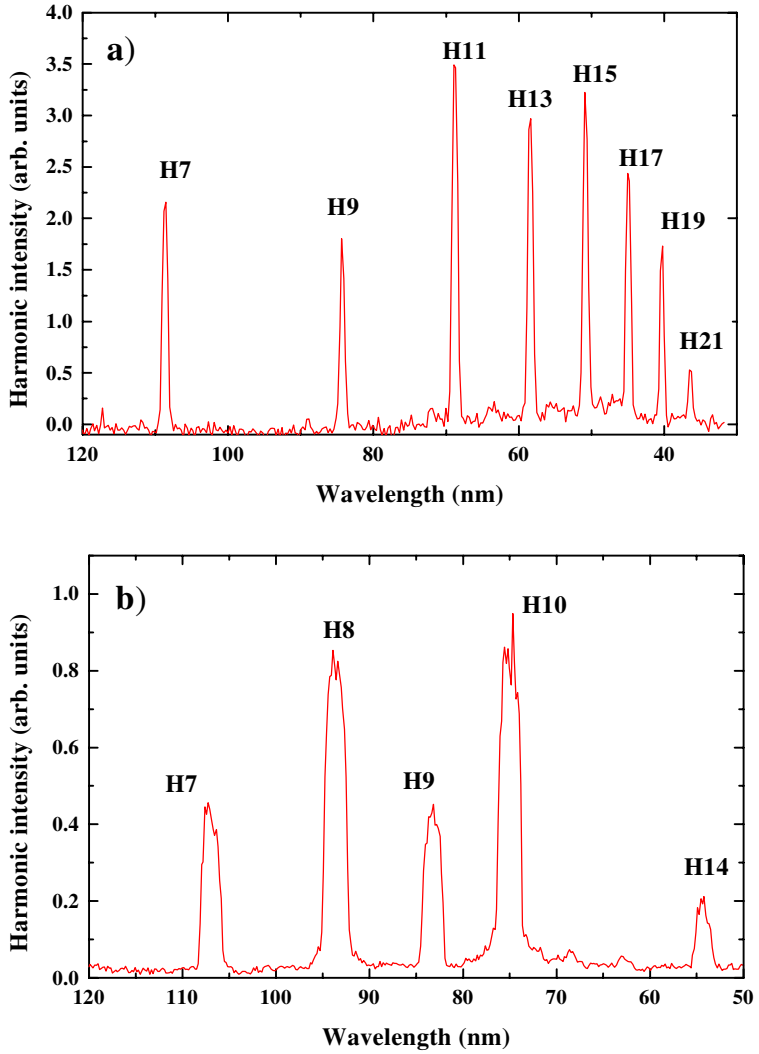

Figure 5.2 *Harmonic spectra generated with (a) the fundamental frequency, and (b) both the fundamental and the doubled frequency of the amplified DFDL.*

nm and in (b) the DFDL is tuned to 752 nm and the light is frequency doubled before harmonic generation. There are a number peaks in the spectrum in (b) that have been generated through a combination of the fundamental and doubled light, making the harmonic spectrum irregular. For example the 8th harmonic (which is not the 4th harmonic of the frequency doubled light) can be obtained with either the combination 6(ω)+1(2ω), or the combination 2(ω)+3(2ω). (Due to parity conditions the total number of photons should be odd.) The 13th harmonic in (a) and the 14th harmonic in (b) were used for spectroscopic measurements reported on in Paper VIII.

5.1.3 Lifetime measurements

There are several ways to experimentally determine the lifetime of an excited state. Below we describe the two methods that have been employed in this thesis: laser-induced fluorescence (LIF) and delayed photo-ionisation pump-probe experiments.

a) Laser-induced fluorescence

A common way to measure lifetimes is to use a laser to excite the atom to the state under investigation. The fluorescence emitted when the atom decays is detected and the lifetime is determined by fitting an exponential to the fluorescence signal. In the most simple case the laser pulse is much shorter than the decay signal and the lifetime can be directly determined from the decay signal. If the duration of the laser pulse is comparable in time to the fluorescence signal a deconvolution between the laser pulse and the detected signal is required to obtain accurate lifetime measurements. The laser pulse should be recorded with the same detection system and under the same conditions as the decay signal. LIF has been used in the studies described in Paper IX and X. In these experiments high-harmonic radiation was not used due to the low excitation energies required. The shortest wavelength required was 195 nm which is generated more efficiently in non-linear crystals.

In paper IX lifetime measurements of an excited state in germanium are discussed. Free germanium atoms were created, and low-lying metastable states populated, in a plasma produced by a 10 ns Nd:YAG laser focused on to a germanium target. Light from the DFDL was frequency tripled in non-linear crystals, and atoms resonantly excited to the state under investigation. The timing between the creation of the plasma and the laser excitation was varied. By waiting until the plasma density was sufficiently low, perturbation free measurements could be made. The fluorescence light was detected in a direction perpendicular to the flight direction of the atoms and the exciting beam. The lifetimes were evaluated by fitting the experimental curves with a convolution of the laser pulse and an exponential curve.

The experimental procedure in Paper X, where the lifetime of an excited state of singly ionised zirconium was measured, presents large similarities with the Ge experiment described above. Zr ions were created in the same way by irradiating a zirconium target with 10 ns laser pulses and excitation was performed with tunable light from the DFDL. The required excitation wavelengths, around 195 nm, were reached by mixing in a non-linear crystal the output from the DFDL with the fourth harmonic of the picosecond Nd:YAG laser. The excitation was performed from low lying metastable states. These states were favourable for lifetime observations since they are present late in the plasma evolution when the temperature and plasma background are lower. Detection and evaluation of the fluorescence was done as described above.

b) Delayed ionisation pump-probe experiments

Using the fluorescence to determine the lifetime, as described above, is a straightforward method, suitable in many cases. However, the emitted wavelength has to be in a suitable wavelength region for efficient detection. In addition, the lifetimes that can be measured by laser-induced fluorescence are limited by the speed of the detection system. Deconvolution of the fluorescence signal can only be done to a certain degree and with decreasing accuracy as the lifetime becomes shorter. For very short lifetimes, shorter excitation pulses are needed, and the electronics are not able to follow the decay signal. For these short lifetimes different pump-probe techniques can be realised, where the time resolution is independent of the detection system. We have measured the lifetimes of some excited states in carbon monoxide employing such a technique. Due to the large excitation energy required we used the 7th harmonic of the amplified DFDL as the pump to excite the state under investigation. The third harmonic of the picosecond Nd:YAG laser probed the population in the excited state by ionising all the molecules in that state. The scheme is illustrated in Figure 5.3. The number of ions created (proportional to the population of the excited state) was detected with a time-of-flight spectrometer (TOF). The TOF can have a collection efficiency of one, which means that all ionised species are detected. A layout of the experimental setup is shown in Figure 5.4. The time delay between the two pulses was varied by manually translating a mirror, so that the decay of the population in the excited state could be observed. The time response of the system is independent of the detection system and is only limited by the duration of the pump and the probe pulses. For short lifetimes the

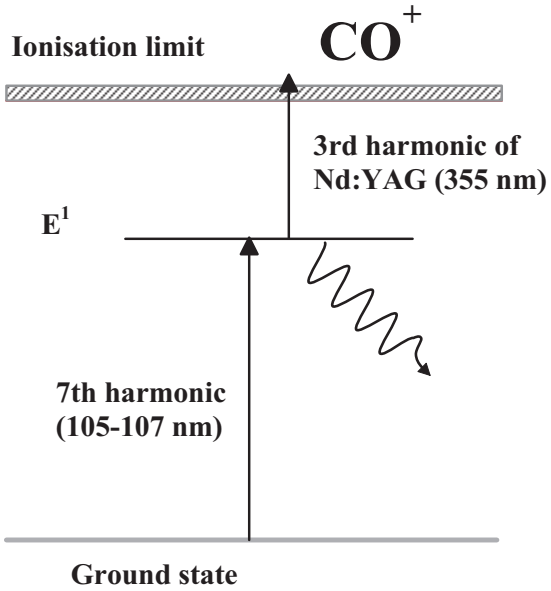

Figure 5.3 *Two-step ionisation of CO. The molecule is excited with the 7th harmonic of the DFDL, and subsequently ionised with the 3rd harmonic of the Nd:YAG laser.*

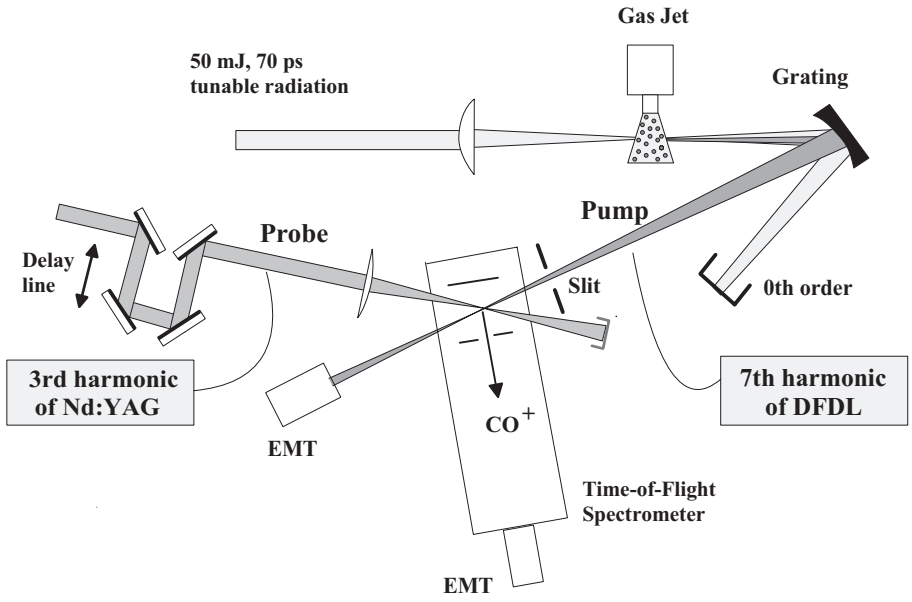

Figure 5.4 *Experimental layout for pump-probe experiments in CO.*

trig jitter of the laser pulses are often significant. To avoid this problem both the pump and the probe originate from the same laser. The aim in this study was to measure the lifetimes of the $E^1\Pi$, v=0 and v=1 states in CO
for different isotopes. The study was motivated by the fact that CO is the second most abundant molecule in the galaxy and a key ingredient in the chemistry of the interstellar medium. Measuring the lifetimes of these excited states allows a determination of the probability of *predissociation*. When a bound state of a molecule couples to a continuum state, there is a certain probability that the molecule will dissociate upon excitation to this state. This phenomenon is called predissociation [66] and will reduce the lifetime of the state. By measuring the lifetimes of the two states in the different isotopes, and using calculated values for the *radiative* lifetimes, we were able to calculate the predissociation probabilities for the different isotopes. We found that the lifetimes are considerably shorter for the v=1 state and vary between the different isotopes. The implications are discussed further in Paper VII.

c) Sources of errors

Although these two methods are examples of direct lifetime measurements, several potential sources of errors do exist.

- **Shortening of the radiative lifetime due to collisions**

If the density is high or the upper state is long-lived there is an increased possibility for the atom or molecule to return to the ground state by radiationless collisions instead of radiative transitions. This will make the radiative lifetime appear shorter

than the true radiative lifetime. To ensure that the measurement is not affected by collisions a study should be made of the lifetime as a function of pressure. If the measurements do not vary, the effect of collisions can be ignored. We performed careful checks to make sure that our measurements were not affected by collisions. In the studies reported in Paper IX and X this was done by varying the plasma density by changing the delay between the ablating laser and the exciting laser, thereby allowing the plasma to expand more. By changing the pressure in the CO experiment (Paper VII) the same examination was performed.

- **Flight-out-of-view**

The detection system generally images a restricted area. If the excited species moves outside the imaged area before it has decayed, the long-lived states will not have the same probability of being detected, thus causing the measured lifetime to appear shorter than the actual lifetime. This effect can be a problem when investigating long lifetimes or species with a high velocity. That the effect is negligible is checked by changing the imaged area and ensuring that the lifetime is not affected.

- **Radiation trapping**

Radiation trapping can occur if the emitted radiation is reabsorbed by neighbouring atoms or molecules. The probability of absorption depends on the transition probability and the number of atoms or molecules available in the lower state. Species in a short-lived state (high oscillator strength) decaying to the ground state (high population) will be especially vulnerable to this effect. Again, changing the pressure or plasma density and measuring the lifetime can clarify if radiation trapping is influencing the measurement.

- **Saturation**

When short lifetimes are measured by fitting a convolution of the laser pulse and the detected signal, care must be taken so that the excitation step is not saturated by the laser pulse. This is avoided by keeping the laser energy sufficiently low. Saturation is not a problem when high-harmonics are used due to the relatively low intensities.

5.1.4 Photo-ionisation cross-sections

Paper VIII reports on measurements of photo-ionisation cross-sections of excited states in helium. The helium atom, having only two electrons, represents an attractive model system for the study of photon-atom interactions. Theoretical calculations are simplified, due to the existence of only two electrons, allowing for theoretical models to be tested and compared with experimental results. The direct ionisation of ground state He atoms has been studied extensively. However, the knowledge about photo-ionisation cross-sections of excited states is limited due to the high excitation energies required presenting severe experimental difficulties.

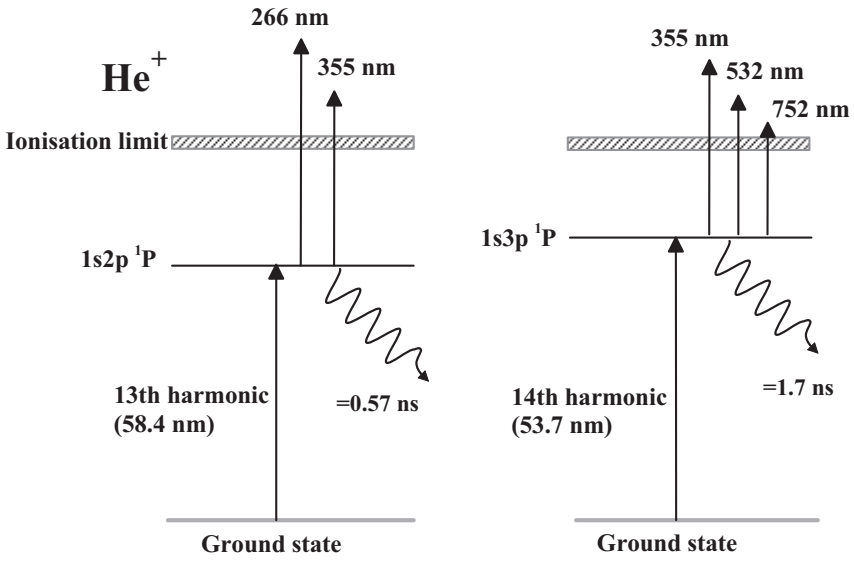

Figure 5.5 *Two-step ionisation pathways in helium with various probe wavelengths.*

We have measured the energy dependence of the photo-ionisation cross-sections (σ_{ion}) of the 1s2p ^{1}P and 1s3p ^{1}P states in He. The high excitation energies of these states, corresponding to photons in the XUV, and the short lifetimes make harmonic radiation, with a narrow bandwidth, suitable as an excitation source. We employ a pump-probe configuration similar to the one described in Figure 5.4. The time delay of the probe is now kept constant whereas the probe wavelength is varied. Although the setup is quite similar to the one described in the previous section this experiment presents added difficulties. Firstly, obtaining absolute values for the ionisation cross-section requires the knowledge of more experimental parameters. Secondly, changing the probe wavelength affects the shape of the focus of the probe making intensity estimates more difficult. These difficulties have been overcome by imaging the focal area of the probe, as well as of the pump, and analysing the shape of the ion signal as function of probe energy.

The two-photon excitation pathways are shown in Figure 5.5. We have used the 13th harmonic (58.4 nm) generated in krypton to excite the 1s2p ^{1}P state. For the 1s3p ^{1}P state the light was frequency doubled before the harmonic radiation was created. The 7th harmonic (53.7 nm) was selected for excitation (i.e. the 14th harmonic of the fundamental). To study the energy dependence of the photo-ionisation cross-section we have chosen a few low-order harmonics of the picosecond Nd:YAG laser, and one additional probe wavelength (752 nm) was obtained by splitting off a small part of the light coming from the DFDL before the final amplification pass in the Ti:sapphire crystal.

Details of the results and our analysis can be found in Paper VIII. To summarise the results, we found a stronger energy dependence for $\sigma_{ion}(1s3p)$ than for $\sigma_{ion}(1s2p)$ in the energy region close to threshold. This is in good agreement with theoretical predictions.

5.2 XUV interferometry

Interferometry is a way of studying the optical properties of materials with high accuracy. By letting two beams interfere in the far field, one can measure optical properties of an object inserted into the optical pathway of one of the beams. The difference in optical path length will introduce a slight shift in the interference fringes; by recording the fringe shift one can measure the optical properties of the object. Plasma interferometry has been demonstrated in the soft X-ray wavelength range using X-ray lasers [67,68], requiring expensive and large setups. The use of harmonic radiation to perform interferometry is interesting largely due to the simplicity and compactness of the harmonic source. Other advantages are the short pulse duration and ability to 'tune' the radiation by choosing different harmonics.

One of the incentives to do interferometry with short wavelengths is the possibility to perform plasma interferometry. Short wavelengths are required due to the large electron densities (N_e) present in a laser produced plasma. A large electron density will give rise to refraction and absorption of light. The critical density, N_{cr}, which is the density at which the plasma strongly refracts and absorbs light, is given by

$$N_{cr} = \frac{1.1\times10^{21}}{\lambda^2} \tag{5.8}$$

where N_{cr} is obtained in cm^{-3} and the wavelength is in μm. From this relation it is clear that a short wavelength is required for penetration of dense plasmas. However, the refractive index, n_{ref}, which is given by

$$n_{ref} = \sqrt{1-\frac{N_e}{N_{cr}}} \tag{5.9}$$

becomes close to one at very high critical densities (i.e. very short wavelengths for a given plasma density). Consequently, there will be a very small fringe shift which will be hard to detect. The optimal wavelength probing the plasma should therefore be short enough to avoid refraction and absorption, but long enough to induce a significant dephasing of the beam propagating through the plasma. One advantage of using harmonic radiation is the possibility to select the optimum wavelength of the radiation by choosing a suitable harmonic. Another advantage is the short pulse duration which allows for temporally resolved studies of fast processes in plasmas.

In this section we discuss the use of harmonic radiation as a source for XUV interferometry. We have demonstrated XUV interferometry, using harmonic radiation, for the first time. Initially, we used the fringe shift to measure the thickness variation of an aluminium filter as a demonstration of the feasibility of the method. In a second step, we applied the technique to determine the spatial variation of the electron density of a laser-produced plasma [Paper V, 69].

To obtain a high temporal resolution the femtosecond Ti:sapphire system was used, providing pulses of 110 fs. The experimental setup, shown in Figure 5.6, is similar to the one used to measure the temporal coherence as described in Chapter 4. The Michelson interferometer now acts as a beam splitter and the two pulses are superimposed in time. Placing the beam splitter in the fundamental and then producing two sources of XUV radiation, rather than using a XUV beam splitter, is a major advantage with our approach, since XUV beam splitters of high quality are extremely difficult to produce.

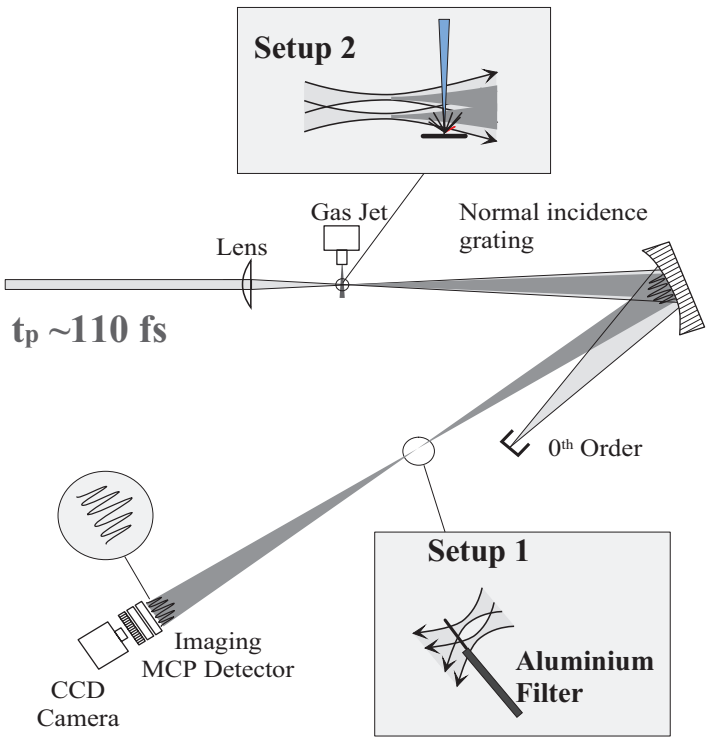

Figure 5.6 *Experimental layout for interferometric measurements. Setup 1 was used to probe a thickness step in an aluminium filter and Setup 2 was used to probe the electron density in a plasma.*

5.2.1 Filter measurements

In **Setup 1** the aluminium filter under investigation was inserted just after the image plane of the two sources (where the beams were still spatially separated). The filter was composed of a 100 nm aluminium layer on top of which a second layer was deposited on half, in order to build a step. We studied the transition region by recording the interference pattern when one beam passed through the thin uniform layer and the other passed through the part containing the step. The shift in fringe position can be seen clearly in Figure 5.7 for the 13th harmonic. The top part of the image is the reference fringe pattern, while the bottom part includes the phase effect due to the larger thickness of aluminium. Cross-sections of the contrast below (grey) and above (black) the transition region are also shown from which the fringe shift can be measured.

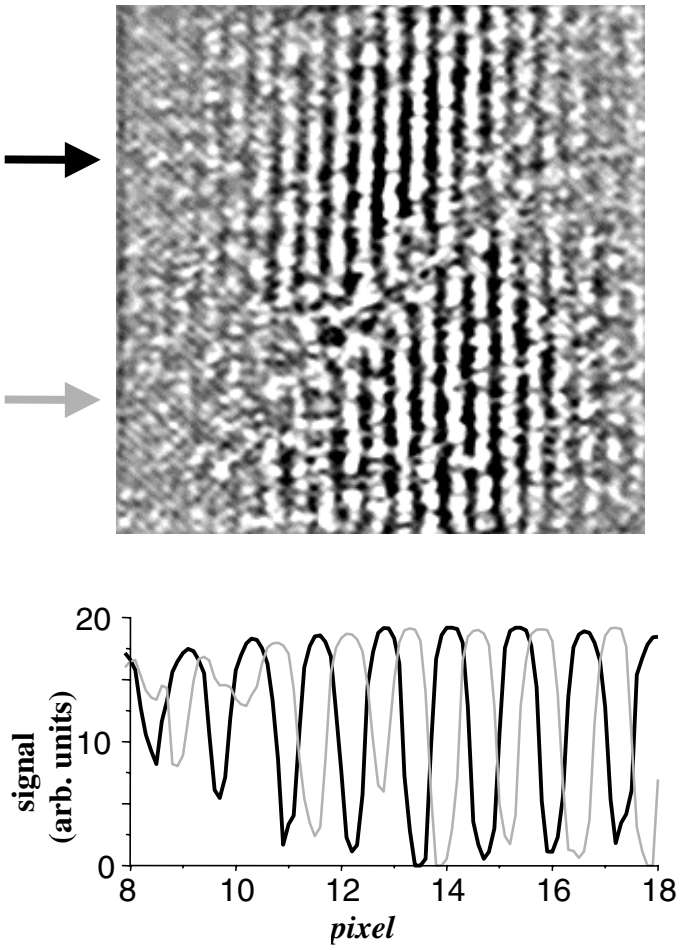

Figure 5.7 *Interference pattern obtained with the 13th harmonic probing an aluminium step filter together with a cross-section of the contrast above (black) and below (grey) the transition region.*

5.2.2 Determination of electron densities in a laser-produced plasma

To take advantage of the high temporal resolution, we probed an expanding laser-produced plasma created on an aluminium target. By placing the plasma directly after the gas jet, as shown in **Setup 2** in Figure 5.6, the amount of light reaching the detector was reduced. Only one of the beams propagated through the expanding plasma. Single-shot interference patterns, using the 11^{th} harmonic, are shown in Figure 5.8, with no plasma (a), and with a plasma present (b). In (b) the fringes are tilted and the noise has increased somewhat due to plasma light, as compared to (a). We estimate the electron densities from the fringe shift and have marked the electron densities corresponding to 0.3, 1 and 2×10^{20} electrons/cm^3 in the figure as dashed lines (highest densities closest to the target). More details and results from the experiment can be found in Paper V.

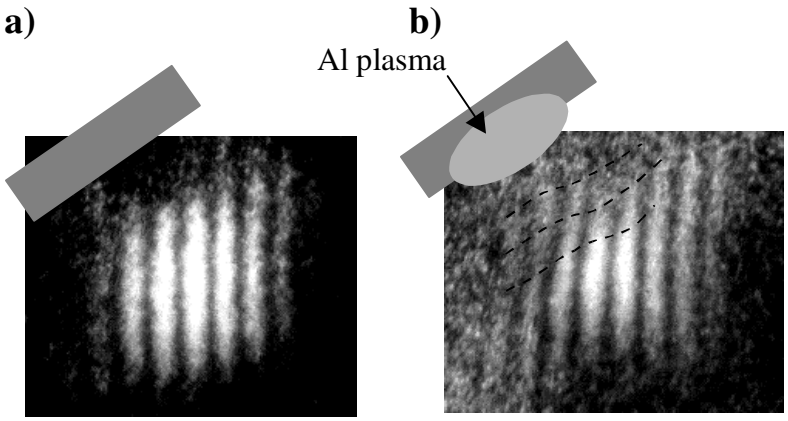

Figure 5.8 *Single-shot interference patterns obtained with the 11^{th} harmonic (a) without plasma and (b) with plasma. Isodensity lines are shown in (b) marking the electron densities at 0.3, 1 and 2×10^{20} electrons/cm^3.*

6. Outlook

Forecasting the impact of high-order harmonic generation is not easy since the field is such a fundamental one. However, there are some areas where the prospects of harmonic generation are particularly promising and unique possibilities exist. Below, a brief outlook into two fields which appear especially promising is given. The first field concerns applications using harmonic radiation, taking advantage of the characteristics where harmonic generation complements other sources. The second field is the generation of attosecond pulses. This is truly an experimental challenge which is expected to lead to the shortest pulses of coherent radiation ever produced.

The work in this thesis is strongly oriented towards applications and it has shown harmonic radiation to be a high quality source, both through the characterisation of the light and the applications performed. The future development of harmonic radiation as a source is intimately connected with the development of high-power laser systems. With the recent development of efficient laser systems, with a kilohertz repetition rate, the flux can be increased significantly which greatly improves usefulness. Further optimisation of the source is of interest and experimental setups dedicated to producing a high photon flux with properties suitable for specific applications should be designed.

This work has described a few applications in **spectroscopy**, where the narrow bandwidth, the high peak power and the short pulse duration of harmonic radiation have been taken advantage of. These are applications especially suited for harmonic radiation. Many applications, now carried out at synchrotron facilities, are likely to be performed using harmonic radiation in the future, either because of the different properties of harmonic radiation as compared with synchrotron radiation or because of the increased availability of the harmonic source.

XUV interferometry using high-harmonic radiation, which has been demonstrated in this thesis, is a promising area where the high temporal resolution can be used to study fast processes. As mentioned in Chapter 5, interferometry with very short wavelengths has been performed, also using X-ray lasers. However, as discussed earlier, harmonic radiation has quite different characteristics. One can expect that the simplicity of the setup, the high repetition rate of the source and the possibility of high temporal resolution will lead to applications in XUV interferometry particularly well suited for harmonic radiation.

One of the special characteristics of harmonic radiation is its intrinsic high peak power, many orders of magnitude higher than that from an undulator at, say 100 eV. In addition, the good spatial properties of harmonic radiation allow for an efficient refocusing into a small spot. Using high-quality XUV focusing optics, where the short pulse length can be maintained, very high intensities should be

attainable in the XUV region. This makes harmonic radiation especially interesting for non-linear processes, where the efficiency of the process is strongly dependent on the peak intensity. **Multiphoton** processes in the XUV region, like multiphoton ionisation or harmonic generation, could therefore become an area of novel applications of this source.

In connection to high-intensity XUV applications, it should be mentioned that the self-amplified-spontaneous-emission (SASE) free electron laser (FEL) [70], being built for example at the DESY laboratory in Hamburg, will open up completely new possibilities for applications using short wavelengths. According to predictions, the peak photon flux will be very high at 10^{26} photons/s (down to 0.1 nm), which is many orders of magnitude higher than is possible to produce with any source available today. The pulse length will be approximately 200 fs which means that the temporal resolution will still be slightly better using high-harmonic radiation. If the SASE FEL fulfils expectations it will be quite superior to harmonic generation for some applications. However, as for high-quality synchrotron beam lines, the availability will be very limited.

The shortest optical laser pulses achieved today are approximately 5 fs [29] and there is a constant striving to achieve even shorter pulses. High-order harmonics are a promising way to generate **attosecond pulses**, i.e. pulses of a duration of only a few hundred attoseconds (1 as=10^{-18} s). The harmonic plateau consists of peaks that are separated equally in frequency with approximately the same amplitude. If the harmonics are locked in phase with each other (i.e. with a constant phase difference between consecutive harmonic orders), the temporal profile will consist of a train of attosecond pulses separated by half the laser period [71,72]. There is a clear similarity to mode-locked lasers where, by locking the different modes oscillating in the laser cavity, trains of very short pulses can be achieved. Uncertainty has existed as to whether the harmonics are emitted in phase. Although the existence of intensity-dependent dipole phases seems to contradict this, Antoine *et al.* [73] showed theoretically that attosecond pulses can still be produced. Despite the harmonics in the plateau not being strictly phase locked, due to the two trajectories having different phase dependencies, one of the contributions can be singled out under certain geometrical conditions. This agrees well with our observations described in Section 4 and in Paper IV.

There are a few different approaches to generating single attosecond pulses discussed in the literature. In one scheme, the attosecond pulse is generated due to harmonic emission being possible only during a very short time. Corkum *et al.* [74] proposed a way of shaping the fundamental pulse to consist of linear polarisation only during a very short time. As harmonic generation is very sensitive to the laser polarisation, harmonic emission will be possible during only this very limited time. In the semi-classical model this corresponds to a single electron – core re-encounter, thus producing an attosecond pulse. Another way to temporally limit the emission is to use an ultra-short, ultra-intense driving laser pulse. Because of the

very fast ionisation due to the rapid rise time of the laser pulse the harmonic emission is again limited to a very short time. Simulations have predicted the generated pulses to be below 500 attoseconds [75].

Although the generation of attosecond pulses is already an experimental challenge, the measurement of the resulting pulse duration will be an even more difficult task. Indirect indications of the pulse duration such as the widening of the spectrum, can be measured relatively easily. Other ways of measuring the pulse length with subfemtosecond resolution are discussed in [76].

With femtosecond pulses it is possible to probe molecular dynamics with temporal resolution. Attosecond pulses would enable even faster processes to be investigated, such as the electron dynamics in an atom, inner-shell electron relaxation processes and ultrafast nuclear motions in light molecules. These extremely short pulses could therefore lead to a new field of research, *attophysics.*

7. Comments on the papers

Paper I High-order harmonic generation from a number of different molecular gases were investigated using 150 fs pulses. A comparison of the conversion efficiency and maximum photon energy was made in different species: rare gases (Ar, Xe), diatomic molecules (N_2, H_2, O_2, CO) and polyatomic molecules (SF_6, N_2O, CO_2, CH_4, C_3H_8).

Paper II We demonstrate that two harmonic sources, generated by two spatially separated sources, are locked in phase. This is done by focusing a picosecond laser into two positions in the gas jet, and studying the interference of the harmonic radiation in the far field.

Paper III The temporal coherence was studied and measured up to the 15^{th} harmonic using a 100 fs laser. We observed two regions, an inner and an outer, in the interference pattern in the far field with different coherence times. The results were interpreted as the result of two different electronic trajectories contributing to harmonic generation.

Paper IV Systematic studies of the temporal coherence were performed up to the 29^{th} harmonic using 110 fs pulses. We showed how the coherence time in the two regions changes as function of harmonic order, laser intensity and focusing conditions. Theoretical simulations were performed, confirming our interpretation of the two regions being a result of different electronic trajectories.

Paper V XUV interferometry was demonstrated for the first time using harmonic radiation. The thickness of an aluminium filter was measured and the electron density of an expanding laser-produced plasma was measured.

Paper VI A picosecond laser system producing narrowband, tunable, radiation from 35 nm to 2 μm is described. Non-linear processes such as high-order harmonic generation and Raman shifting have been employed to cover the wide spectral range.

Paper VII Lifetimes of excited states in CO were measured using high-harmonic radiation. Different isotopes ($^{12}C^{16}O$, $^{13}C^{16}O$ and $^{13}C^{18}O$) that are of astrophysical interest, were examined.

Paper VIII Absolute photo-ionisation cross sections of excited states in He (1s2p ^{1}P and 1s3p ^{1}P) were measured using high-harmonic radiation. The region close to the He^+ 1s ^{2}S threshold (0 to 2 eV) was studied.

Appendix

Paper IX Radiative lifetimes were measured in excited states of Ge using a laser-produced plasma subjected to selective laser excitation. Together with measurements of the branching ratios, oscillator strengths of astrophysical interest were derived.

Paper X Lifetime measurements were performed in excited states of singly ionised Zr, populated in a laser-produced plasma. Combined with measurements of branching ratios the oscillator strengths were determined.

Contributions by the author to the different papers

I contributed to the experimental work described in Paper I-V and VII-IX, with special emphasis on Paper I, III and IV. The experiment described in Paper III was performed in Florence by myself and one of the coauthors from LENS (Florence). I was also in charge of the tunable picosecond laser system used in the experiments described in Papers VI-X. I was first author and responsible for Papers I, IV and VI and I also contributed to the manuscripts of Paper II, III, VII and VIII. The numerical simulations in Paper II-IV have been done by one of the coauthors. The sections related to combustion physics and to the generation of infra-red radiation in Paper VI have been prepared by the coauthors.

Acknowledgements

This work is really the result of a team effort and would have been impossible without the stimulating collaboration with the people at the Division of Atomic physics. I would like to thank everybody who has been involved in some way. In particular I would like to mention the following people:

My supervisor, Claes-Göran Wahlström, who with his broad knowledge of physics has given me guidance through this work. His experimental skill and rational explanations have been much appreciated.

Anne L'Huillier, who with her insight into harmonic generation has been a source of inspiration and a pleasure to work with.

Sune Svanberg, who with his positive spirit and visions can inspire anyone.

Anders Persson, who can fix anything from double pulses to crashed computers and has usually done it before you have asked.

Mette Gaarde for friendship, encouragement and all those words of wisdom.

Jörgen Larsson for sharing some of the tricks of the DFDL and stimulating discussions.

Dominique Descamps and Christian Delfin for good collaborations and discussions.

Marco Bellini and Ted Hänsch, for pleasant and fruitful collaborations both in Florence and in Lund.

Mattieu Gisselbrecht and Michael Meyer, who were a pleasure to work with despite constant battles with the lasers during the helium experiment. Many late nights were spent in the lab that finally proved worth the effort.

Wim Ubachs, Patrice Cacciani and Paul Hinnen, for efficient and enjoyable collaborations during the CO experiment.

Anne Dederichs for all the encouragement and friendship during frustrating moments.

Family and friends, for being there, showing an interest in my work and putting up with my constant lack of time.

My parents who, although usually being very far away, always manage to support and inspire. And, of course, for the lanwidge kårreksjons.

Ellen, for all those valuable (and expensive!) phone calls.

And finally, Kurt, for making these last few years so enjoyable and the last few months possible.

References

[1] A. McPherson, G. Gibson, H. Jara, U. Johann, T.S. Luk, I.A. McIntyre, K. Boyer and C.K. Rhodes, *Studies of multiphoton production of vacuum-ultraviolet radiation in the rare gases,* J. Opt. Soc. Am. B **4**, 595 (1987).

[2] M. Ferray, A. L'Huillier, X.F. Li, L.A. Lomprè, G. Mainfray and C. Manus, *Multiple-harmonic conversion of 1064 nm radiation in rare gases,* J. Phys. B **21**, L31 (1988).

[3] P. Agostini, F. Fabre, G. Mainfray and G. Petite*, Free-free transitions following six-photon ionization of xenon atoms,* Phys. Rev. Lett. **42**, 1127 (1979).

[4] L. DiMauro and P. Agostini, *Ionization dynamics in strong laser fields,* Adv. At. Mol. Opt. Phys. **35**, 79 (1995).

[5] S.-Y. Chen, A. Maksimchuk and D. Umstadter, *Experimental observation of relativistic nonlinear Thomson scattering,* Nature **396**, 653 (1998).

[6] M. Protopapas, C.H. Keitel and P.L. Knight, *Atomic physics with super-high intensity lasers,* Rep. Prog. Phys. **60,** 389 (1997).

[7] C.J. Joshi and P.B. Corkum, *Interactions of ultra-intense laser light with matter,* Physics Today, January 1995.

[8] M.D. Perry and G. Mourou, *Terawatt to petawatt subpicosecond lasers,* Science **264**, 917 (1994).

[9] L.V. Keldysh, *Ionization in the field of a strong electromagnetic wave,* Zh. Eksp. Teor. Fiz **47**, 1945 (1965) [Sov. Phys. JETP **20**, 1307 (1965)].

[10] E. Mevel, P. Breger, R. Trainham, G. Petite, P. Agostini, A. Migus, J.-P. Chambaret and A. Antonetti, *Atoms in strong optical fields: Evolution from multiphoton to tunnel ionisation,* Phys. Rev. Lett. **70,** 406 (1993).

[11] S. Backus, C.G. Durfee, M.M. Murnane and H.C. Kapteyn, *High power ultrafast lasers,* Rev. Sci. Instr. **69**, 1207 (1998).

[12] P.M.W. French, *The generation of ultrashort laser pulses,* Rep. Prog. Phys. **58**, 169 (1995).

[13] D. Strickland and G. Mourou, *Compression of amplified chirped optical pulses,* Opt. Commun. **56**, 219 (1985).

[14] S. Svanberg, J. Larsson, A. Persson and C.-G. Wahlström, *Lund high-power laser facility –Systems and first results,* Phys. Scr. **49**, 187 (1994).

[15] J.J. Macklin, J.D. Kmetec and C.L. Gordon III, *High-order harmonic generation using intense femtosecond pulses,* Phys. Rev. Lett. **70**, 766 (1993).

[16] A. L'Huillier and Ph. Balcou*, High-order harmonic generation in rare gases with a 1-ps 1053-nm laser,* Phys. Rev. Lett. **70**, 774 (1993).

[17] C.-G. Wahlström, J. Larsson, A. Persson, T. Starczewski, S. Svanberg, Ph. Balcou and A. L'Huillier, *High-order harmonic generation in rare gases with an intense short-pulse laser,* Phys. Rev. A **48**, 4709 (1993).

[18] J.L. Krause, K. J. Schafer and K.C. Kulander, *High-order harmonic generation from atoms and ions in the high intensity regime,* Phys. Rev. Lett. **68**, 3535 (1992).

[19] K.S. Budil, P. Salières, A. L'Huillier, T. Ditmire and M. D. Perry, *Influence of ellipticity on harmonic generation,* Phys. Rev. A **48**, R3437 (1993).

[20] Y. Liang, S. Augst, S.L. Chin, Y. Beaudoin and M. Chaker, *High harmonic generation in atomic and diatomic molecular gases using intense picosecond laser pulses –a comparison,* J. Phys. B **27**, 5119 (1994).

[21] C.-G. Wahlström, S. Borgström, J. Larsson and S.-G. Pettersson, *High-order harmonic generation in laser-produced ions using a near-infrared laser,* Phys. Rev. A **51**, 585 (1995).

[22] T.D. Donnelly, T. Ditmire, K. Neuman, M.D. Perry and R.W. Falcone, *High-order harmonic generation in atom clusters,* Phys. Rev. Lett. **76**, 2472 (1996).

[23] P.A. Norreys, M. Zepf, S. Moustaizis, A.P. Fews, J. Zhang, P. Lee, M. Bakarezos, C.N. Danson, A. Dyson, P. Gibbon, P. Loukakos, D. Neely, F.N. Walsh, J.S. Wark and A.E. Dangor, *Efficient extreme UV harmonics generated from picosecond laser pulse interactions with solid targets,* Phys. Rev. Lett. **76**, 1832 (1996).

[24] S. Kohlweyer, G.D. Tsakiris, C.-G. Wahlström, C. Tillman and I. Mercer, *Harmonic generation from solid-vacuum interface irradiated at high laser intensities,* Opt. Commun. **117,** 431 (1995).

[25] K. J. Schafer, B. Yang, L.F. DiMauro and K.C. Kulander, *Above threshold ionization beyond the high harmonic cutoff,* Phys. Rev. Lett. **70**, 1599 (1993).

[26] P.B. Corkum, *Plasma perspective on strong-field multiphoton ionization,* Phys. Rev. Lett **71,** 1994 (1993).

[27] S.G. Preston, A. Sanpera, M. Zepf, W.J. Blyth, C.G. Smith, J.S. Wark, M.H. Key, K. Burnett, M. Nakai, D. Neely and A.A. Offenberger*, High-order harmonics of 248.6-nm KrF laser from helium and neon ions,* Phys. Rev. A **53**, R31 (1996).

[28] Z. Chang, A. Rundquist, H. Wang, M.M. Murnane and H. Kapteyn, *Generation of coherent soft x rays at 2.7 nm using high harmonics,* Phys. Rev. Lett. **79,** 2967 (1997).

[29] Ch. Spielmann, N.H. Burnett, S. Sartania, R. Koppitsch, M. Schnürer, C. Kan, M. Lenzner, P. Wobrauschek and F. Krausz, *Generation of coherent X-rays in the water window using 5-femtosecond laser pulses,* Science **278**, 661 (1997).

[30] P. Lambropoulos, *Mechanisms for multiple ionization of atoms by strong pulsed lasers,* Phys. Rev. Lett. **55**, 2141 (1985).

[31] T. Ditmire, J.K. Crane, H. Nguyen, L.B. DaSilva and M.D. Perry, *Energy-yield and conversion-efficiency measurements of high-order harmonic radiation,* Phys. Rev. A **51**, R902 (1995).

[32] Ph. Balcou, C. Cornaggia, A.S.L. Gomes, L.A. Lomprè and A. L'Huillier, *Optimizing high-order harmonic generation in strong fields,* J. Phys. B **25**, 4467 (1992).

[33] Ph. Balcou and A. L'Huillier, *Phase matching effects in strong field harmonic generation,* Phys. Rev. A **47**, 1447 (1993).

[34] M. Lewenstein, P. Salières and A. L'Huillier, *Phase of the atomic polarisation in high-order harmonic generation,* Phys. Rev. A **52,** 4747 (1995).

[35] P. Salières, A. L'Huillier and M. Lewenstein, *Coherence control of high-order harmonics,* Phys. Rev. Lett. **74**, 3776 (1995).

[36] P. Salières, A. L'Huillier, Ph. Antoine and M. Lewenstein, *Study of the spatial and temporal coherence of high order harmonics,* Adv. At. Mol. Opt. Phys. **41**, 83 (1999).

[37] A. Rundquist, C.G. Durfee III, Z. Chang, C. Herne, S. Backus, M.M. Murnane and H.C. Kapteyn, *Phase-matched generation of coherent soft X-rays,* Science **280**, 1412 (1998); C.G. Durfee III, A.R. Rundquist, S. Backus, C. Herne, M.M. Murnane and H.C. Kapteyn, *Phase matching of high-order harmonics in hollow waveguides,* Phys. Rev. Lett. **83**, 2187 (1999).

[38] E. Constant, D. Garzella, P. Breger, E. Mevél, Ch. Dorrer, C. Le Blanc, F. Salin and P. Agostini, *Optimizing high harmonic generation in absorbing gases: Model and experiment,* Phys. Rev. Lett. **82**, 1668 (1999).

[39] Y. Tamaki, Y. Nagata, M. Obara and K. Midorikawa, *Phase-matched high-order harmonic generation in a gas-filled hollow fibre,* Phys. Rev. A **59** 4041 (1999).

[40] Y. Tamaki, J. Itatani, Y. Nagata, M. Obara and K. Midorikawa, *Highly efficient, phase-matched high-harmonic generation by a self-guided laser beam,* Phys. Rev. Lett. **82,** 1422 (1999).

[41] C. Altucci, T. Starczewski, E. Mevél, C.-G. Wahlström, B. Carré and A. L'Huillier, *Influence of atomic density in high-order harmonic generation,* J. Opt. Soc. Am. B **13**, 148 (1996).

[42] A. Bouhal, R. Evans, G, Grillon, A. Mysyrowicz, P. Berger, P. Agostini, R.C. Constantinescu, H.G. Muller and D. von der Linde*, Cross-correlation measurement of femtosecond noncollinear high-order harmonics*, J. Opt. Soc. Am. B **14**, 950 (1997).

[43] T.E. Glover, R.W. Schoenlien, A.H. Chin and C.V. Shank, *Observation of laser assisted photoelectric effect and femtosecond high order harmonic radiation,* Phys. Rev. Lett. **76**, 2468 (1996).

[44] M.E. Faldon, M.H.R. Hutchinson, J.P. Marangos, J.E. Muffet, R.A. Smith, J.W.G. Tisch and C.G. Wahlström, *Studies of time-resolved harmonic generation in intense laser fields in xenon,* J. Opt. Soc. Am. B **9**, 2094 (1992).

[45] T. Starczewski, J. Larsson, C.-G. Wahlström, J.W.G. Tisch, R.A. Smith, J.E. Muffet and M.H.R. Hutchinson, *Time-resolved harmonic generation in an ionizing gas*, J. Phys. B **27**, 3291 (1994).

[46] J.W.G. Tisch, R.A. Smith, J. E. Muffett, M. Ciarrocca, J.P. Marangos and M.H.R. Hutchinson, *Angularly resolved high-order harmonic generation in helium*, Phys. Rev. A **49** R28 (1994).

[47] J.W.G. Tisch, D.D. Meyerhofer, T. Ditmire, N. Hay, M.B. Mason and M.H.R. Hutchinson, *Measurement of the spatiotemporal evolution of high-order harmonic radiation using chirped laser pulse spectroscopy*, Phys. Rev. Lett. **80** 1204 (1998).

[48] P. Salières, T. Ditmire, K.S. Budil, M.D. Perry and A. L'Huillier, *Spatial profiles of high-order harmonics generated by a femtosecond Cr:LiSAF laser,* J. Phys B **27** L217 (1994).

[49] J.E. Muffet, C.-G. Wahlström and M.H.R. Hutchinson, *Numerical modelling of the spatial profiles of high-order harmonics,* J. Phys. B **27**, 5693 (1994).

[50] T. Ditmire, E.T. Gumbrell, R.A. Smith, J.W.G. Tisch, D.D. Meyerhofer and M.H.R. Hutchinson, *Spatial coherence measurement of soft X-ray radiation produced by high order harmonic generation,* Phys. Rev. Lett. **77**, 4756 (1996).

[51] A.E. Siegman, *Lasers* (University Science Books, California, 1986).

[52] M. Lewenstein, Ph. Balcou, M.Yu. Ivanov, A. L'Huillier and P.B. Corkum, *Theory of high-harmonic generation by low-frequency laser fields,* Phys. Rev. A **49**, 2117 (1994).

[53] K.C. Kulander, K.J. Schafer and J.L. Krause, *Time-dependent studies of multiphoton processes,* in *Atoms in Intense Radiation Fields*, edited by M. Gavrila (Academic Press, New York, 1992).

[54] M.B. Gaarde, Ph. Antoine, A. L'Huillier, K.J. Schafer and K.C. Kulander, *Macroscopic studies of short-pulse high-order harmonic generation using the time-dependent Schrödinger equation,* Phys. Rev. A **57**, 4553 (1998).

[55] Ph. Antoine, D.B. Milošević, A. L'Huillier, M.B. Gaarde, P. Salières, and M. Lewenstein, *Generation of attosecond pulses in macroscopic media,* Phys. Rev A **56**, 4960 (1997).

[56] K.J. Schafer and K.C. Kulander, *High harmonic generation from ultrafast pump lasers*, Phys. Rev. Lett. **78**, 638 (1997).

[57] M.B. Gaarde, F. Salin, E. Constant, Ph. Balcou, K.J. Schafer, K.C. Kulander and A. L'Huillier, *Spatiotemporal separation of high harmonic radiation into two quantum path components,* Phys. Rev. A **59**, 1367 (1999).

[58] R. Haight and D. Peale, *Antibonding state on the Ge(111):As surface: spectroscopy and dynamics,* Phys. Rev. Lett. **70**, 3979 (1993).

[59] W. Theobald, R. Häßner, C. Wülker and R. Sauerbrey, *Temporally resolved measurement of electron densities ($>10^{23}$ cm^{-3}) with high harmonics*, Phys. Rev. Lett. **77**, 298 (1996).

[60] J. Larsson, E. Mevel, R. Zerne, A. L'Huillier, C.-G. Wahlström and S. Svanberg, *Two-colour time-resolved spectroscopy of helium using high-order harmonics,* J. Phys B **28,** L53 (1995).

[61] A. L'Huillier, T. Auguste, Ph. Balcou, B. Carré, P. Monot, P. Salières, C. Altucci, M.B. Gaarde, J. Larsson, E. Mevel, T. Starczewski, S. Svanberg, C.-G. Wahlström, R. Zerne, K.S. Budil, T. Ditmire and M.D. Perry, *High-order harmonics: A coherent source in the XUV range,* Int. J. Nonlinear Opt. **4,** 647 (1995).

[62] P. Erman, A. Karawajczyk, E. Rachlew-Källne, E. Mevel, R. Zerne, A. L'Huillier and C.-G. Wahlström, *Autoionization widths of the NO Rydberg-valence state complex in the 11-12 eV region,* Chem. Phys. Lett. **239**, 6 (1995).

[63] S.L. Sorensen, O. Björneholm, S. Buil, D. Descamps, T. Kihlgren, A. L'Huillier, J. Norin, G. Öhrwall, S. Sundin, S. Svensson and C.-G. Wahlström, *Femtosecond pump-probe photoelectron spectroscopy of predissociative Rydberg states in acetylene,* to be published.

[64] C.V. Shank, J. E. Bjorkholm and H. Kogelnik, *Tunable distributed-feedback dye laser,* Appl. Phys. Lett. **18**, 395 (1972).

[65] W. Schade, B. Garbe and V. Helbig, *Temperature tuned distributed feedback dye laser with high repetition rate,* Appl. Opt. **29**, 3950 (1990).

[66] G. Herzberg, *Spectra of Diatomic Molecules* (Robert E. Krieger Publishing Company, Malabar, Florida, 1989).

[67] L.B. Da Silva, T.W. Barbee, Jr., R. Cauble, P. Celliers, D. Ciarlo, S. Libby, R.A. London, D. Matthews, S. Mrowka, J.C. Moreno, D. Ress, J.E. Trebes, A.S. Wan and F. Weber, *Electron density measurements of high density plasmas using soft x-ray laser interferometry,* Phys. Rev. Lett. **74**, 3991 (1995).

[68] F. Albert, D. Joyeux, P. Jaeglé, A. Carillon, J.P. Chauvineau, G. Jamelot, A. Klisnick, J.C. Lagron, D. Phalippou, D. Ros, S. Sebban and P. Zeitoun, *Interferograms obtained with a X-ray laser by means of a wavefront division interferometer,* Opt. Comm. **142**, 184 (1997).

[69] H. Merdji, P. Salières, L. Le Déroff, J.-F. Hergott, B. Carré, D. Joyeux, D. Descamps, J. Norin, C. Lyngå, A. L'Huillier, C.-G. Wahlström and M. Bellini, *Coherence properties of high-order harmonics: Application to high-density laser-plasma diagnostic,* submitted (1999).

[70] B.H. Wiik, *The TESLA project: an accelerator facility for basic science,* Nucl. Inst. and Methods in Physics A **398**, 1 (1997).

[71] S.E. Harris, J.J. Macklin and T.W. Hänsch, *Atomic scale temporal structure inherent to high-order harmonic generation,* Opt. Commun. **100**, 487 (1993).

[72] Gy. Farkas and Cs. Tóth, *Proposal for attosecond light pulse generation using laser induced multiple-harmonic conversion processes in rare gases,* Phys. Lett. A **168**, 447 (1992).
[73] Ph. Antoine, A. L'Huillier and M. Lewenstein*, Attosecond pulse trains using high-order harmonics*, Phys. Rev. Lett. **77**, 1234 (1996).
[74] P.B. Corkum, N.H. Burnett and M.Y. Ivanov, *Subfemtosecond pulses,* Optics Lett. **19** 1870 (1994).
[75] I.P. Christov, M.M. Murnane and H.C. Kapteyn, *High-harmonic generation of attosecond pulses in the "single-cycle" regime,* Phys. Rev. Lett. **78**, 1251 (1997).
[76] E. Constant, V.D. Taranukhin, A. Stolow and P.B. Corkum, *Methods for the measurement of the duration of high-harmonic pulses,* Phys. Rev. A **56**, 3870 (1997).